PROMOTioN
PROGRESS ON MESHED HVDC OFFSHORE TRANSMISSION NETWORKS

Report D15.3 Report on DC GIS diagnostic and monitoring tools and methods

PROMOTioN – Progress on Meshed HVDC Offshore Transmission Networks
Mail info@promotion-offshore.net
Web www.promotion-offshore.net

This result is part of a project that has received funding form the European Union's Horizon 2020 research and innovation programme under grant agreement No 691714.

CONTACT

Cornelis Plet – DNV GL
cornelis.plet@dnvgl.com
Uwe Riechert – ABB Switzerland Ltd
uwe.riechert@ch.abb.com

DOCUMENT INFO SHEET

Document Name: Report on DC GIS diagnostic and monitoring tools and methods
Responsible partner: TU Delft
Work Package: WP 15
Work Package leader: Uwe Riechert
Task: 15.3
Task lead: Armando Rodrigo Mor – TU Delft

DISTRIBUTION LIST

APPROVALS

	Name	Company
Validated by: Task leader: WP Leader:	 Armando Rodrigo Mor Uwe Riechert	 TU Delft ABB Switzerland Ltd

DOCUMENT HISTORY

Version	Date	Main modification	Author
1.0	26-11-2018	TU Delft	Armando Rodrigo Mor
2.0			

WP Number	WP Title	Person months	Start month	End month
15	HVDC GIS Technology Demonstrator	164.5	23	48

Deliverable Number	Deliverable Title	Type	Dissemination level	Due Date
15.3	Report on DC GIS diagnostic and monitoring tools and methods	Report	Public	M30

LIST OF CONTRIBUTORS

Work Package and deliverable involve a large number of partners and contributors. The names of the partners, who contributed to the present deliverable, are presented in the following table.

PARTNER	NAME
TU Delft	Armando Rodrigo Mor, Luis Castro Heredia, Fabio Andres Muñoz
ABB	Uwe Richert, Michael Gatzsche
DNV GL	Hong He, Konstantinos Dimitropoulos, Cornelis Plet
SHE Transmission	Yash Audichya
SGI	Thanh Vu, Alain Girodet
TenneT	Kees Korman

CONTENT

NOMENCLATURE

ABBREVIATION	EXPLANATION
HVAC	High Voltage Alternating Current
HVDC	High Voltage Direct Current
GIS	Gas Insulated System / Switchgear
PD	Partial Discharge
PRPD	Phase-resolved PD Pattern
HFCT	High Frequency Current Transformer
RF	Radio Frequency
UHF	Ultra High Frequency
VHF	Very High Frequency
D15.3	PROMOTioN deliverable 15.3
WP	Working package

EXECUTIVE SUMMARY

PROMOTioN WP 15 aims to realize a DC GIS Technology Demonstrator that ultimately leads to increase the Technology Readiness Level (TRL) for HVDC GIS. Several cornerstone tasks have been defined to achieve such a goal, which include research on Monitoring and Diagnostics techniques (M&D) for HVDC GIS.

As an important part of M&D, the measurements of PD (partial discharges) are used worldwide by GIS manufacturers and utilities for detection of incipient defects in the insulation system of GIS, for which different radio-frequency (RF) techniques have been the main measuring method.

The partial discharge event produces electromagnetic waves that are measured by the RF techniques in several frequency ranges, that according to the IEC62478 include the VHF (very high frequency: 30MHz – 300MHz) and the UHF (ultra-high frequency: 300MHz – 3000MHz). At the present time, the UHF method is the most extensively used method to measure PD activity because is less sensitive to noise and easier to handle in comparison with the IEC270 conventional method. This technique is relatively simple: it uses a coupling sensor (antenna) to extract the UHF signals that are excited within the GIS by short bursts of PD pulses and a digital acquisition system that condition, filter and process the electrical signal. The GIS enclosure acts as a Faraday cage, shielding the antenna from electromagnetic interference disturbances and enabling a low background noise level, which result in a high sensitivity of the UHF method.

Despite the VHF/UHF methods provide high immunity to noise and high sensitivity, they also present some disadvantages such as low spatial sensitivity and no correlation to the PD event current. The RF signal attenuation is large within a few meters, therefore manufacturers have to provide the GIS with multiple antennas to increase the sensitivity of the measuring system. In addition, attenuation, distortion and filtering of the RF signal makes it no possible to quantify the magnitude of the PD event at the source.

Although the balance of advantages and limitations of RF techniques is still positive, this WP has foreseen alternative techniques and methods to complement and that may downplay the limitations of RF techniques. In this report corresponding to deliverable D15.3, the experimental results for alternative PD measuring systems in the low frequency range are presented. A different approach has been researched in the course of this W15, that makes use of HFCT sensors. This technique was proven to boost spatial sensitivity and relationship with the PD source.

This project has received funding from the European Union's Horizon 2020 research and innovation programme under grant agreement No 691714.

1 INTRODUCTION

1.1 MOTIVATION

PROMOTioN aims to increase the Technology Readiness Level (TRL) for HVDC GIS, which means that the perspectives for the DC GIS technology are to soar in the short or medium term. An increase of renewable sources especially offshore will yield a higher demand for DC GIS technology and in turn, this implies increasing demands on components, materials and M&D tools.
Currently, only few HVDC GIS are in operation worldwide. In consequence, little service experience and few information about the long-term capability of this type of technology are available. Additionally, there are no international standards established for specifying and testing such systems. WP 15 is set off to tackle this lack of laboratory and field experience as a way to anticipate oncoming needs.
The efforts as part of the D15.3 are to be focused on several levels such as:

- Laboratory Level. Contribution to the methods, techniques, knowledge and understanding of PD phenomena with laboratory test-cells.
- Component Level. Testing of a PD measuring system on an actual GIS to validate the proof of concept.

1.2 RELATION TO PROMOTION

This document serves as the third deliverable D15.3 of work package WP15 “DC GIS technology demonstrator”. Furthermore, it falls under task 15.2. “Develop monitoring and diagnostic method and applicability of SF6 alternatives” which is led by TU Delft (The Netherlands).

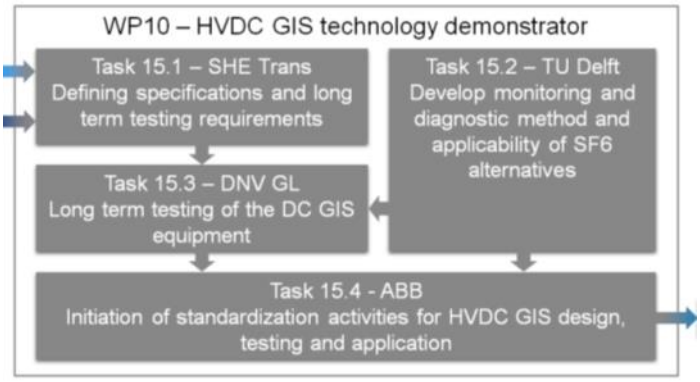

Deliverables

- D15.1 : Document on recommendations for specifying DC GIS systems (SHE Trans, M30)
- D15.2 : Document on test requirements, procedures and methods (DNV GL, M30)
- D15.3 : Report on DC GIS diagnostic and monitoring tools and methods (TU Delft, M36)
- D15.4 : Anonymized test reports on tests carried out (DNV GL, M48) - Classified
- D15.5 : Report of diagnostic analysis and condition assessment (TU Delft, M48)
- D15.6 : White- and position papers on pre-standardization of DC GIS testing (DNV GL, M48)
- D15.7 : Report on characteristics of PD Alternative gas: comparison with SF6 (SGI, M36)
- D15.8 : Report on long term monitoring of DC GIS with defects (SGI, M48)

This project has received funding from the European Union’s Horizon 2020 research and innovation programme under grant agreement No 691714.

2 PARTIAL DISCHARGE M&D OF GIS SYSTEMS

Gas Insulated Systems as any other component of the high voltage network demands monitoring and diagnostics (M&D) techniques in seek of the high reliability required to achieve the expected service life of around 30 and 40 years. Failure to do so leads to expensive outages and shutdowns of industrial processes. However, M&D actions are only taken after an economical and technical analysis of every asset. As reported in [1], a survey by the CIGRE Joint Working Group 33/23.12 found a dielectric failure rate of 0.9 per 100 bay-years for GIS installed between 1967 and 1992. A second survey 5 years later still reported a total failure frequency of 0.75 failures per 100 bay-years. A more recent survey by CIGRE WG A3.06 [2] covering 2004-2007 showed that the overall major failure rate for GIS bays is about 0.37 major failures per 100 GIS bay-years of service.
These all statistics support the need of effective on-site partial discharge M&D techniques in order to achieve the required high reliability and service life.
In order to monitor dielectric defects in the GIS that can lead to failure or breakdown, on-line PD monitoring systems are available and has been applied extensively for decades. They can help in the identification of defects such as:

- particle on enclosure (free moving)
- particle on insulating material
- protrusion on conductor
- protrusion on enclosure
- floating conducting part
- void in insulating material
- delamination of insulation from electrode
- cracks in insulation material

Conventionally an on-line GIS PD system relies on the VHF/UHF technique, using antennas to pick up the electromagnetic radiation created by a PD event. The post processing of the recorded PD pulses tipically leads to create patterns that reveal the nature of the PD source and assist in the action-taking process.

Documents such as the IEC TS 62478 [3] and CIGRE WG. D1.25 [4] defines a “sensitivity check” as a means to verify that a VHF/UHF measuring system on-field is able to pick up signals equivalent to 5 pC as measured by the conventional IEC 60270 method during laboratory tests. Field experience supports that the VHF/UHF systems are sensitive and high resilient to noise due to the high frequency range at which they record signals. In addition, the high cost of a tipical GIS repair together with the consequent cost of supply disruption usually outweigh the initial cost of a PD monitoring system.

This project has received funding from the European Union’s Horizon 2020 research and innovation programme under grant agreement No 691714.

On the other hand, the IEC TS 62478 also summarizes three possible disadvantages of VHF/UHF systems, namely:

- Not possible to calibrate the magnitude of the PD in terms of its apparent charge (pC).
- Higher cost compared to conventional IEC PD systems since the technique necessarily operates at higher frequencies stepping up the requirements of hardware.
- Extra cost because their sensors are not for generic purpose, but specifically for the GIS to be deployed instead.

It is important to highlight that the knowledge about HVDC is far away from the present knowledge in HVAC. Additionally, the PD mechanism, measurements, and recognition are not directly comparable with the PD under AC voltage. Many studies have been conducted about partial discharges in DC voltage using different parameters such as the type of gas and its pressure, voltage, and type of defect [5]–[9]. These studies have addressed the most relevant challenges to the HVDC technologies as the transition from Trichel discharges to Glow discharges, the development of classification techniques and evaluating methods to assess HVDC components by means of PD measurements, the sensitivity and the vertical range of the measurement systems, and the measuring of partial discharges in the pulseless region.

In HVAC, the PRPD is a powerful tool to classify and evaluate the partial discharges occurring in HV components. Nevertheless, in DC there is no such a powerful tool available due to the lack of a phase angle for the PD pulses, which means that there are only two basic parameters available to classify and evaluate the partial discharges: the discharge magnitude and the time of occurrence. Besides, as is mentioned in [9] “compared to the standardized methods for the AC PD measurement (IEC 60270) with related evaluation methods (PRPD Pattern etc.) there are no useful testing procedures and meaningful acceptance criteria defined to assess HVDC components, especially for GIS and GIL.”

Another important topic to be addressed in further investigations is the transition between Trichel pulses to glow discharges under DC voltage, because this transition has shown to be the border between a region where the PD pulses can be detected by electrical methods and a region where the pulses are only detectable by optic methods. The region where the pulses cannot be detected by electrical methods is known as “pulseless” region. In this region, there is a strong ionization of the gas and high density of charge carriers causing a conduction current that cannot be measured by the conventional electric methods.

This project has received funding from the European Union’s Horizon 2020 research and innovation programme under grant agreement No 691714.

These disadvantages caused this WP to research alternatives to the former drawbacks. The first year of research conducted by the WP 15 has resulted in concepts for an HFCT-based measuring system that mainly contributes the following features:

- Increased spatial sensitivity.
- Potential for correlation to the PD quantities at its source.

In this report, the experiments involved in the proof of concept of the HFCT-based measuring system were conducted applying mainly AC voltage. Results applying DC voltage will be reported in the second deliverable D15.5.

This project has received funding from the European Union's Horizon 2020 research and innovation programme under grant agreement No 691714.

3 MAIN TASKS

In the course of this first year of execution of WP 15, TU Delft has developed concepts for a PD measuring system, that unlike RF methods, makes use of HFCT sensors to measure the induced current of the PD events that flows along the GIS compartments. Since no other works have been published on a similar matter, the development of the measuring system concepts has demanded preparation and modifications of the components involved at both hardware and software level.
Although this document focuses on reporting the experimental results of the proof of concept, several underlaying tasks were carried out in the process. These activities included:

3.1 HARDWARE SPECIFICATION FOR PARTIAL DISCHARGE MEASUREMENTS

3.1.1 PREPARATION OF TEST OBJECTS

Tests and results will be collected from several different test-objects.

Test Object	User	Description	Role in this report
1	TU Delft	Actual size HVAC GIS including bushing, switchgear, T-connectors, and ground switch.	Main tests. Results are fully reported in D15.3.
2	TU Delft	Test cells to produce and measure PD in laboratory.	Main tests. Results are fully reported in D15.3.
3	TU Delft/SGI	DC laboratory-sized GIS	Secondary tests. Some results are reported in D15.3.
4	TU Delft/ABB	Actual HVDC GIS.	Secondary tests. Results are not included in D15.3 since these tests are scheduled for 2019.

The test results in section 4.2 to 4.6 all refer to the measurements carried out with test objects 1 and 2, which means that these two test objects play the major role in this report.

Test object 3 is a laboratory-size HVDC GIS located at SuperGrid Institute. Results from this test object are secondary and were used to verify the functioning of the HFCT-based system. Results from test object 3 are reported in section 4.7.

The test object 4 located at DNV-GL Laboratory was equipped with HFCT sensors intended to monitor the GIS during the long term testing that deliverable D15.2 refers to. This test object 3 is

This project has received funding from the European Union's Horizon 2020 research and innovation programme under grant agreement No 691714.

ready for the long term testing scheduled for 2019 and is only included in this report in section 4.8 to describe one of the software tools developed for PD acquisition.

3.1.2 PREPARATION OF SENSORS

The developed measuring system has been designed to measure PD activity in GIS, therefore the HFCT sensors demanded specific preparation to meet the requirements. One of the novelties of the measuring system is that it measures the induced current of the PD events as it flows along the GIS compartments. To pick up these currents the sensors have to meet these requirements:

- High gain and broad bandwidth. These features anabled to pick up the very small signals that were expected with sufficiently bandwidth to resolve the pulse in time domain.
- HFCT Case. The sensors to be used were designed and built by TU Delft so that they fit into the physical dimensions of the test object 1. This is a major subject in the report D15.3 since the installation of the HFCT makes use of the bolts that connects mechanically and electrically two adjacent compartments.
- Amplifiers/filters. Signal acquisition was a challenge due to the small magnitude of the PD pulses. Amplifiers and filters were also designed and built when needed.

3.1.3 PREPARATION OF THE ACQUISITION SYSTEM.

The developed measuring system is a broadband system intended for time domain acquisition of PD signals. This determined the requirements of the acquisition system, which included:

- Selecting suitable acquisition systems. Tektronix and NI systems were tested to find their suitability for this application.
- Collection of requirements for data acquisition.
- Write Labview/Matlab code for data acquisition.

3.2 TESTING OF PARAMETERS FOR MONITORING AND DIAGNOSTICS

The validation of the measuring system included a series of test measurements to determine experimentally the following concepts:

- Pulse distribution. Several laboratory measurements were conducted to prove that the PD current flows along the compartment and bolts and that the current distribution is

This project has received funding from the European Union's Horizon 2020 research and innovation programme under grant agreement No 691714.

homogeneous provided the path impedances are symmetric. This proved the HFCT measuring method.

- PD current attenuation along the GIS. By using HFCT, the measuring technique is focused on the low-frequency range of the PD current, which is less attenuated as it travels along the GIS compartments. This principle resulted in the ability of the system to detect PD pulses meters away from the PD source.

- PRPD patterns. The phase-resolved PD patterns from each of the test cells were measured and compared to the reference patterns available in literature. This method was used to validate the performance of the measuring system.

- VHF/UHF vs HFCT. The report will also be focused on the performance comparison between RF techniques and our HFCT technique, with particular attention to sensitivity and attenuation.

3.3 SOFTWARE FOR DATA ACQUISITION AND DATA ANALYSIS

The measuring system performs all of the analysis by software, relying on hardware exclusively for data acquisition. Thus, the report includes a description of the following software tools:

- LabView acquisition software. This code is the software that is used for testing on test object 4. During the development of Task 15.3, TU Delft is to provide a version of the measuring system to run parallel to the long term testing at DNV-GL. Results if available by the submission date of report D15.3 will be included.

- Matlab postprocessing software. A proprietary software (PDflex) developed by TU Delft is updated, modified and extended to perform the calculations established as requirements for the M&D system.

This project has received funding from the European Union's Horizon 2020 research and innovation programme under grant agreement No 691714.

4 PD MEASUREMENTS ON GIS USING HFCT SENSORS

With the growing trend towards HVDC GIS technology, testing with DC voltages, development of evaluating tools such as NODI patterns as an alternative for PRPD patterns [10] and new measuring techniques are gaining renewed relevance. In the field of measuring techniques, the optical detection is a technique that has caught attention due to its resilience to noise and ability to detect glow-less PD signals that usually cannot be detected by electrical methods.

Amongst alternative measuring systems and techniques currently in development, this WP presents a PD measuring technique which makes use of HFCT sensors. The proposed technique measures the current induced in the GIS enclosure by the PD phenomena. The HFCTs are installed conveniently at the bolts of spacers, in such a way that they are able to measure the current travelling along the GIS compartments. Unlike the UHF antennas, the HFCT does not measure the electromagnetic field in the insulation, but the induced currents in the enclosure by a PD event.

The electromagnetic waves produced by a PD pulse propagate in a GIS structure as in a coaxial transmission line, where each GIS component such as spacers, L branches, T joints, circuit breakers, etc., has his own electromagnetic behavior. Therefore, the PD pulses suffer from attenuation, reflections and dispersion as they travel along the different components. Nevertheless, different researchs [cita] have shown that the damping and dispersion is significantly higher in the VHF and UHF range.

Accordingly, the bandwidth of the HFCT sensors used in the experiments was chosen from hundreds of kHz to a few hundreds of MHz, low frequency range where the attenuation due to the GIS components is relatively smaller in comparison to the VHF and UHF range [11]. Therein lies the potential of this measuring technique. Taking advantage of this lower attenuation, the measuring system here introduced aims to offer an increased spatial sensitivity as compared to VHF/UHF systems.

Experimental results and substantial information contained in the following sections were extracted from the journal paper “A Novel Approach for Partial Discharge Measurements on GIS using HFCT Sensors” accepted for publication in the special issue “UHF and RF Sensor Technology for Partial Discharge Detection” in Sensors, 2018.

This project has received funding from the European Union’s Horizon 2020 research and innovation programme under grant agreement No 691714.

4.1 SENSOR ARRANGEMENT

The PD pulse electromagnetic wave includes transverse electric (TE) and transverse magnetic (TM) modes in addition to the transverse electric and magnetic (TEM) mode. At low frequency (up to hundreds of MHz) the TEM mode is predominant, whereas at high frequencies, the TE11 is the most significant mode with a cut off frequency in the range of hundreds of MHz[11][12][13].

The propagation in higher order modes is highly attenuated and distorted. For instance, in [14] is reported that the damping of the PD pulse is frequency-dependent, with frequency components above 500 MHz remarkably damped by spacers, T-shape branches and E-bends.

In a GIS system, partial discharges radiate electromagnetic waves in a frequency spectrum ranging from DC to GHz. These electromagnetic waves induce fast surface currents in the main conductor and in the external enclosure. The PD surface current flows along the compartments, the electrical paths in the spacers, the L branches, T joints, circuits breakers or any other electrical path in the GIS while suffering from attenuation, reflections, and dispersion. This phenomenon is depicted in Figure 1a.

In Figure 1a is also shown that a spacer is placed in between two compartments. The PD pulse creates a surface current that travels along the compartments and bridges the spacer via the installed bolts as depicted in Figure 1b, which connect adjacent compartments [15]. It is important to remark that the bolts are not in electrical contact with the flange of the compartments, therefore the current flows along the bolts. Worth mentioning that the PD current pulse will not be drifted away from the sensor even if there is a grounding point right at the sensor location because the transmission line structure of the GIS offers a path of lower impedance than the grounding path. A HFCT installed at one of the bolts picks up the magnetic field produced by the PD currents. The HFCT measures a portion of the PD currents since they split over the total amount of bolts. The washers and nuts act like bridges closing the path between the bolts and the compartments.

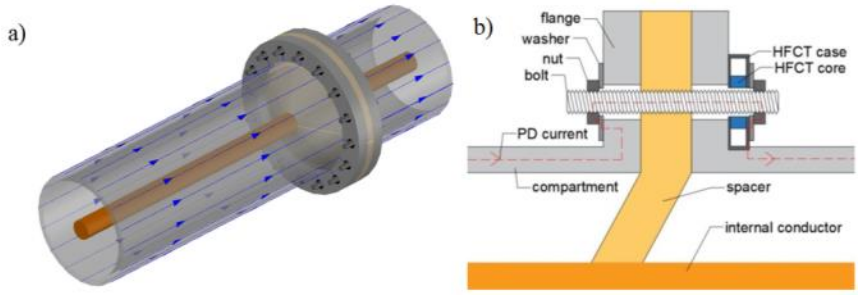

Figure 1. (a) PD pulse currents as they travel along the GIS; (b) PD pulse current flowing along the bolts connecting two compartments.

4.2 TEST OBJECT AND SET-UP

The experiments reported in section 4.2 to 4.6 were conducted on a 380 kV, SF_6, actual-size, gas insulated system available at the High Voltage Laboratory of TU Delft, see Figure 2. This GIS has multiple spacers, T-joints, an earth switch, a switchgear, a bushing and a disconnector. This GIS is

This project has received funding from the European Union's Horizon 2020 research and innovation programme under grant agreement No 691714.

also grounded at several locations including grounding points at the ends and distributed along the compartments. Seven HFCT sensors were installed at the spacers that are shown with yellow labels. The UHF antennas used in the experiments are also indicated with blue labels.

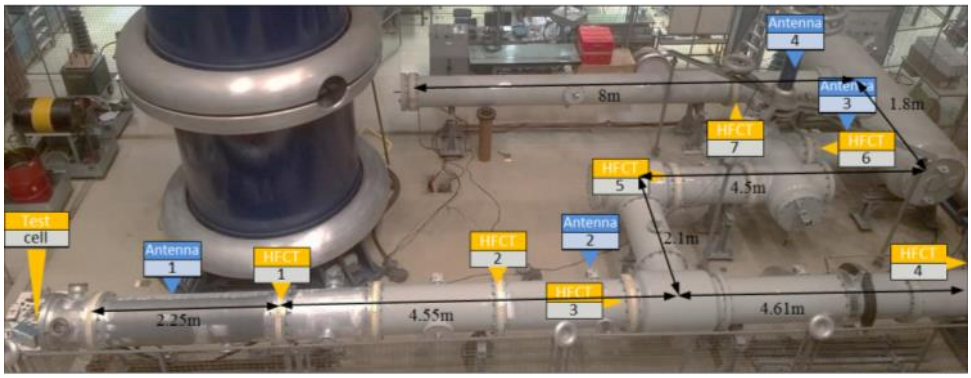

Figure 2. GIS Photograph showing the location of UHF and HFCT sensors.

A set of three test cells were built to produce corona, surface and free moving particle discharges. These test cells can be seen in Figure 3.

Figure 3. (d) corona test cell; (e) free particle test cell; (f) surface test cell.

To hold the test cells along the conductor axis, as depicted in Figure 4, a special arragenment was given to the GIS end. The test cell ground electrode is connected to the enclosure using a lid, see Figure 4a, with multiple current return paths. In the rod holding the test cell, an HFCT is installed as is shown Figure 4b to measure the current produced by the PD. The test cell was replaced with a rod and a proper connector during the experiments with calibration signals as can be seen in Figure 4c.

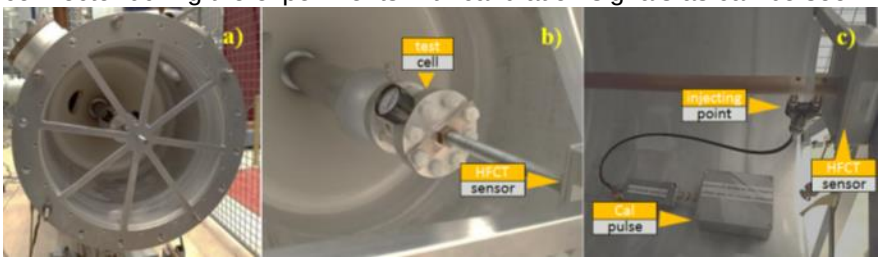

Figure 4. GIS end, (a) ground electrode; (b) positioning of the test cell and sensor; (c) positioning of pulse calibrator.

This project has received funding from the European Union's Horizon 2020 research and innovation programme under grant agreement No 691714.

4.3 HFCT SENSOR

The HFCT sensor depicted in Figure 5a was chosen as the most suitable option to measure the PD current along the bolts because its high gain, its low cut-off frequency, its upper frequency in the range of a few hundreds of MHz and its mechanical properties.

Figure 5. (a) HFCT installed at the GIS; (b) construction of the HFCT sensor; (c) sensor frequency response.

The HFCT teardown is shown in Figure 5b and its frequency response is depicted in Figure 5c, highlighting a gain of 9.1 mV/mA and a bandwidth from 62 kHz to 136 MHz.

In HFCT designs the bandwidth and the gain are cross-related parameter, where a small number of turns increases the gain but decreases the bandwidth [16]. For this application, the requirements of the bandwidth were priority over the gain. Amplifiers were added to the sensors output to step up the sensitivity of the system. The secondary winding of the HFCT sensor comprised five turns wound onto a N30 ferrite core [17]. The five turns were stripes of 3 mm copper tape wound evenly distributed onto the core. The sensor has been equipped with an extra BNC connector, that when short-circuited connects the secondary of the HFCT to the GIS enclosure.

4.4 PD PULSE CURRENT DISTRIBUTION IN GIS

In Figure 1b, it is shown an HFCT sensor installed at one of the bolts of the GIS spacer. Although from the mechanical point of view this arrangemet might require some modifications or specific dimensions for the sensor housing, it also serve the most convenient option in terms of current sensitivity. The reason for this is that the spacer bolts constitutes also the current path with least inductance. Consider that the PD pulse flows in the inner conductor and the compartment along the shortest loop. Any current path drifting away from the main conductor necessarily results in a bigger loop and in turn in a bigger inductance. This effect was checked by installing the HFCT sensor externally to the bolt forming two different loops and injecting a pulse at the location illustrated by Figure 4c. In addition, the bolt was replaced with an insulating bolt so the current was pushed to flow along the external loop. A comparison of the results is seen in Figure 6.

This project has received funding from the European Union's Horizon 2020 research and innovation programme under grant agreement No 691714.

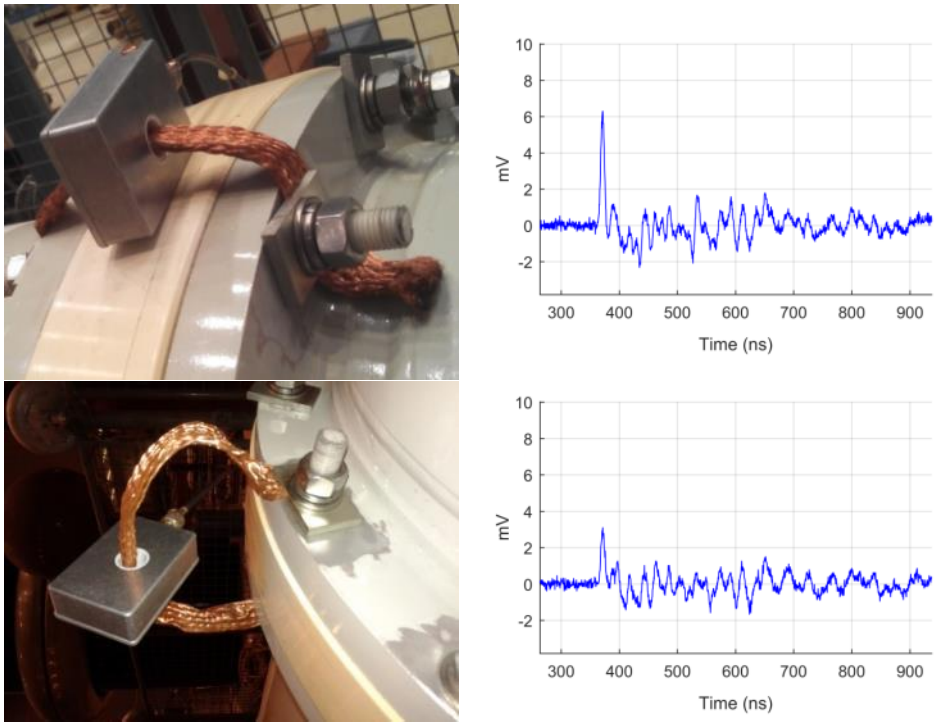

Figure 6. Effect of current path length on the signal amplitude, (a) short current path, (b) long current path.

The peak amplitude of the measured pulses confirmed that the bigger loop yields to a bigger inductance and in consequence, the measured signal is smaller compared to the case when the loop was made shorter. On the other hand, these results yield to other important finding: the several ground connections possible in a GIS do not affect the current passing along the HFCT sensors because they also entails ground paths of much higher inductance than the inductance of the main conductor-compartment arrangement. Experiemental results demonstrated that the amplitude of the signal measured by the HFCT does not change when a grounding point is connected next to the sensor.

Given the former results, then the most suitable installation of the sensors is in the bolts as illustrated in Figure 5a. Once the sensor installation was established, several laboratory measurements were conducted to check the feasibility of this measuring arrangement and to determine the current distribution amongst the bolts of the spacer.

The experiements consisted of injecting a fast pulse by using a calibrator located at the GIS end and measure the response of one or several HFCT located at spacer 1 (2.25m away from the injection point). Bolts having no sensors installed were unchanged or given dielectric washers to prevent any current from flowing along them. A summary of each measurement configuration is shown below in Table 1.

This project has received funding from the European Union's Horizon 2020 research and innovation programme under grant agreement No 691714.

Table 1. Description of the sensor arrangement installed at spacer 1.

	Configuration 1	Configuration 2	Configuration 3a	Configuration 3b
Sensors installed	1	4	4	1
Number of bolts acting as current paths	15	12	0	0

4.4.1 CONFIGURATION 1

In Figure 6, both the injected and the measured signal are shown, where it is possible to notice that the HFCT 1 picked up 5.43% of the peak value of the injected signal. Considering the 16 bolts as current paths, theoretically 6.25% of the injected current should flow along each bolt, however the HFCT installed added an extra impedance to that current path causing the small deviation between the measured signal and the theoretical value.

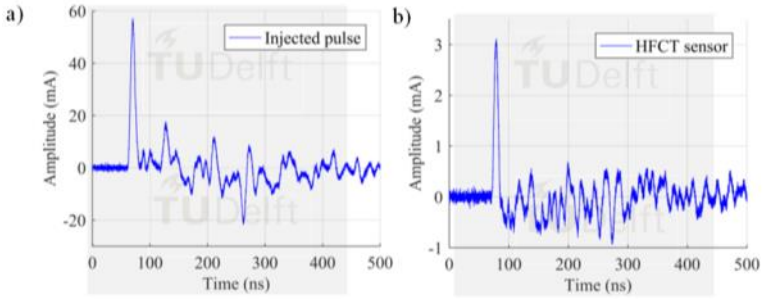

Figure 6. Configuration 1, (a) pulse injected at the test cell position; (b) pulse measured by HFCT 1. Only one sensor installed and 15 parallel current paths.

4.4.2 CONFIGURATION 2

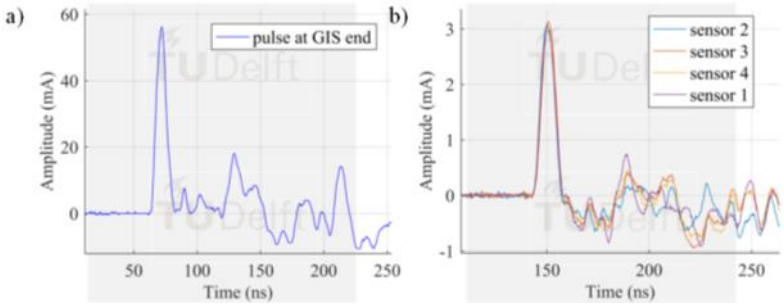

Figure 7. Configuration 2, (a) pulse injected at the test cell position; (b) pulses measured by HFCT 1. Four sensors installed and 12 current paths (remaining bolts).

With this configuration, the ratio of the peak amplitudes was 5.51%, similar to that achieved by configuration 1. Moreover, the similarity in pulse shape and peak amplitude of the measured pulses, showed in Figure 7b, proved that the pulse current flows homogenously along the GIS compartment perimeter.

This project has received funding from the European Union's Horizon 2020 research and innovation programme under grant agreement No 691714.

4.4.3 CONFIGURATION 3

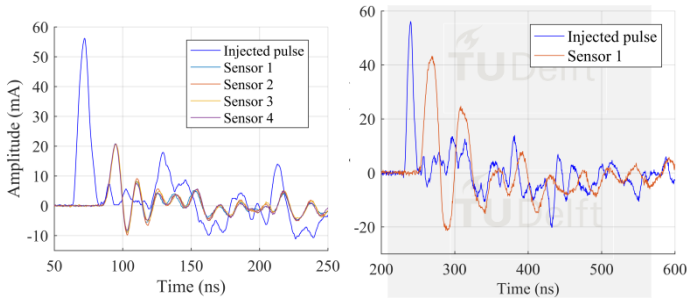

Figure 8. Configuration 3, pulse injected at the test cell position (a) four sensors installed and no current flowing through the remaining 12 bolts; (b) one sensor installed and no current flowing through the remaining 15 bolts.

Several differences were found in these results as compared to the two previous configurations. First, the current amplitude measured at each sensor was 37% of the amplitude of the injected pulse at the GIS end. This ratio is significantly higher than the limit assuming that the pulse current is to be split into the 4 sensors which would result ideally in a ratio of 25%. Second, the pulse shape measured by the sensors featured an undershoot not seen in the previous configurations. These results are explained as the distortion caused by the large impedance change. In configuration 1 and 2, the amount of parallel conducting bolts was predominantly bigger than the amount of bolts with sensors. The effect of the sensors was reduced and the measured amplitudes fit reasonably the simple model of the input current being split into the number of current paths. In this last case of study, the change of impedance by adding more sensors and reducing the remaining current paths led to reflections that distorted the shape of the measured pulses.
An additional evidence is presented in Figure 8b. In this case, just one sensor was left and the remaining 15 bolts were given dielectric washers. The distortion of the measured pulse is such that its peak amplitude is around 70% of the injected pulse amplitude. Furthermore, it shows a significant distortion, with undershoot and pulse width increase.

According to the results of the experiments, the installation of HFCT sensors at the spacers proved to be feasible to pick up signals flowing along the GIS compartments. Although configuration 3 yields to a higher sensitivity, configuration 1 will be the preferred one because the effect of reflections is minimum as compared to other configurations.
In the following sections, measurements with PD test cells are carried out to study the performance of HFCT installed at the spacers as a measuring system.

This project has received funding from the European Union's Horizon 2020 research and innovation programme under grant agreement No 691714.

4.5 PERFORMANCE ANALYSIS

The performance of the HFCT-based measuring system to detect typical PD defects was researched by analyzing the signals from sensors distributed in the GIS. Type, location, amplification and bandwidth of these sensors are given in Table 2.

Table 2. Testing parameters used in each test cell.

	Corona	Surface	Free particle
HFCT Test cell	Sensor: 5 mV/mA, BW 3.92 kHz-1.11 GHz Amp: 26dB, BW 100 kHz-1.3 GHz		Sensor: 9.1 mV/mA, BW 62 kHz-136 MHz
HFCT 1	Sensor: 9.1 mV/mA, BW 62 kHz-136 MHz Amps: 21.7dB, 27 kHz-955 MHz + 25.1dB, 24 kHz-1.14 GHz		Sensor: 9.1 mV/mA, BW 62 kHz-136 MHz Amp: 25.1dB, 24 kHz-1.14 GHz
HFCT 3	Sensor: 9.1mV/mA, BW 62 kHz-136 MHz Amps: 22.7dB, 30 kHz-1.23 GHz + 25.3Bb, 23 kHz-1.23 GHz		Sensor: 9.1 mV/mA, BW 62 kHz-136 MHz Amp: 22.7dB, 30 kHz-1.23 GHz
HFCT 6	Sensor: 9.1mV/mA, BW 62 kHz-136 MHz Amps: 21.7dB, 27 kHz-955 MHz + 25.1dB, 24 kHz-1.14 GHz		Sensor: 9.1 mV/mA, BW 62 kHz-136 MHz Amp: 25.1dB, 24 kHz-1.14 GHz
HFCT 7	Sensor: 9.1mV/mA, BW 62 kHz-136 MHz Amps: 22.7dB, 30 kHz-1.23 GHz + 25.3Bb, 23 kHz-1.23 GHz		Sensor: 9.1 mV/mA, BW 62 kHz-136 MHz Amp: 22.7dB, 30 kHz-1.23 GHz
Antenna 1	Sensor: VHF/UHF Amps: 25.1dB, 21 kHz-1.21 GHz + 25.3dB, 23 kHz-1.23 GHz		Sensor: VHF/UHF Amp: 25.1dB, 24 kHz-1.14 GHz
Antenna 2	Sensor: VHF/UHF Amps: 25.5dB, 23 kHz-1.15 GHz + 25.3dB, 23 kHz-1.23 GHz		Sensor: VHF/UHF 25.3dB, 23 kHz-1.23 GHz
Antenna 3	Sensor: VHF/UHF Amps: 25.1dB, 21 kHz-1.21 GHz + 25.3dB, 23 kHz-1.23 GHz		Sensor: VHF/UHF Amps: 25.1dB, 21 kHz-1.21 GHz + 25.3dB, 23 kHz-1.23 GHz
Antenna 4	Sensor: VHF/UHF Amps: 25.5dB, 23 kHz-1.15 GHz + 25.3dB, 23 kHz-1.23 GHz		Sensor: VHF/UHF Amps: 25.5dB, 23 kHz-1.15 GHz + 25.3dB, 23 kHz-1.23 GHz
AC Test voltage	15 kV_{RMS}	15 kV_{RMS}	12 kV_{RMS}
SF_6 Pressure	3 Bar	3 Bar	2 Bar

This project has received funding from the European Union's Horizon 2020 research and innovation programme under grant agreement No 691714.

For this performance checking, the sensor at the test cell was used as the trigger of the oscilloscope and all the signals were recorded simultaneously. Charge calculation was performed according to [18][19] and not in compliance with IEC60270. Details of the circuit developed to acquire the phase of the PD pulses can be found in [17]. The analysis of the signals from the HFCTs and the comparison with the antennas are reported in the following chapters. Prior to the performance analysis, the PRPD patterns for each defect are shown next.

4.5.1 PRPD PATTERNS OF TEST CELLS

Artificial defects reproducing corona, surface and free moving particle discharges were created. Results, reported in Figure 9, show that representative PRPD patterns were recorded for each different type of defect.

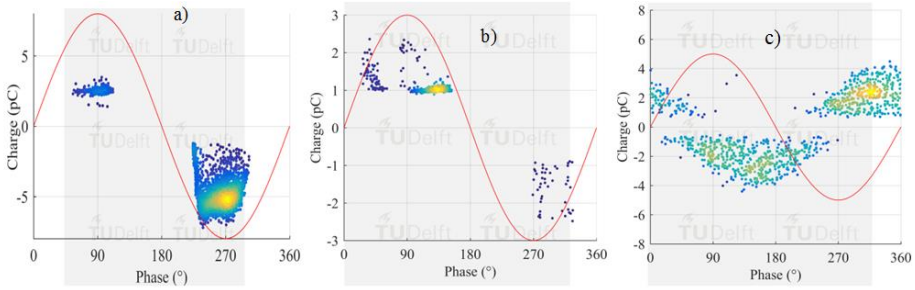

Figure 9. (a) Corona discharge; (b) Surface discharge; (c) Free moving particle.

The test voltage and SF_6 pressure were adjusted for each test cell to produce small discharges, in the range of a few pC, suitable to check the performance of the proposed measuring system. Small magnitudes in the order of 1 to 6 pC were attained.

4.5.2 SENSITIVITY CHECK

The sensitivity attainable by the measuring system in configuration 1 was determined by its ability to pick up the signals corresponding to the PD tests reported in Figure 9. The smallest and the largest signal from each PD test measured by the test cell HFCT were chosen as the reference and the measured signal by the antenna 1 and HFCT 1 were compared. Details of the VHF/UHF sensors can be found in [20].

Figure 10 shows the smallest signal from the corona, surface and free particle discharge test and their corresponding frequency spectrum measured at the test cell. An indication of the magnitude in pC after integration of the current signal [18] is also given.

This project has received funding from the European Union's Horizon 2020 research and innovation programme under grant agreement No 691714.

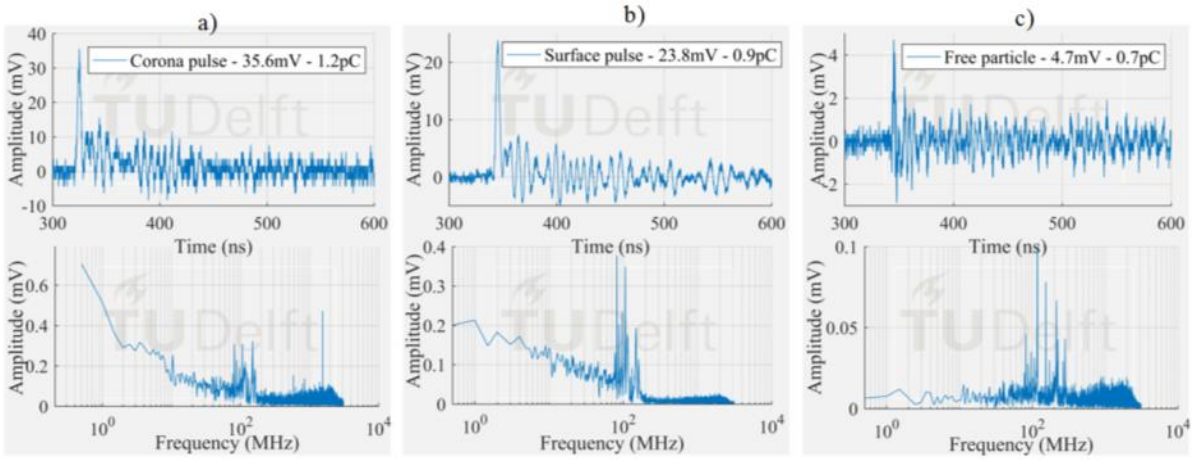

Figure 10. Smallest pulse at the test cell (a) corona; (b) surface; (c) free moving particle.

The voltage signals corresponding to the smallest PD pulses in Figure 9 measured by the antenna 1 and HFCT 1 are observed in Figure 11 to 13.

The corona signal can be distinguished in the VHF range and by the HFCT 1 but not in the UHF range. In the UHF range, the signal from the antenna is affected by the noise picks appearing at around 850 MHz.

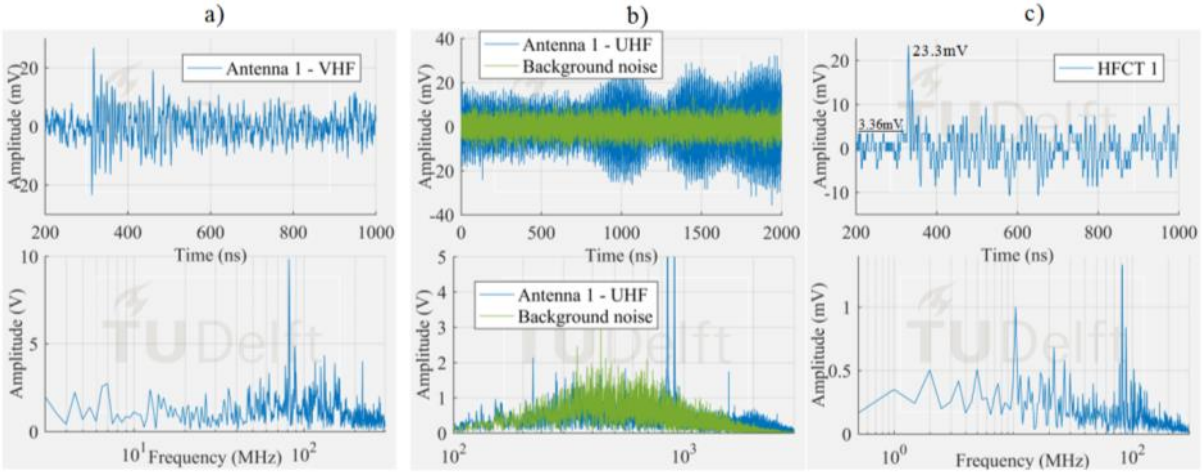

Figure 11. Smallest corona **s**ignal measured by (a) antenna 1 in VHF; (b) antenna 1 in UHF; (c) HFCT 1.

This project has received funding from the European Union's Horizon 2020 research and innovation programme under grant agreement No 691714.

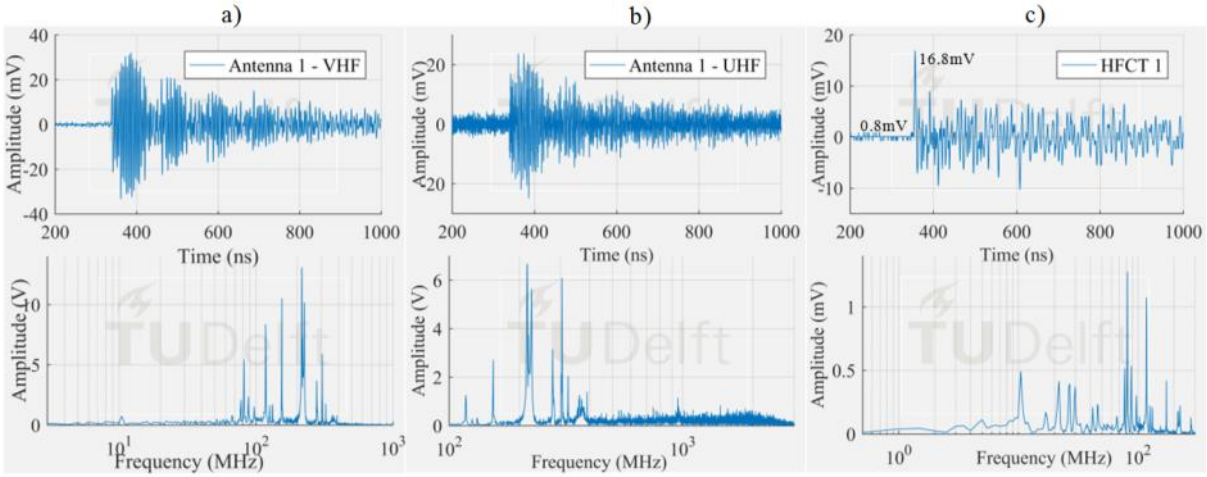

Figure 12. Smallest free particle signal measured by (a) antenna 1 in VHF; (b) antenna 1 in UHF; (c) HFCT 1.

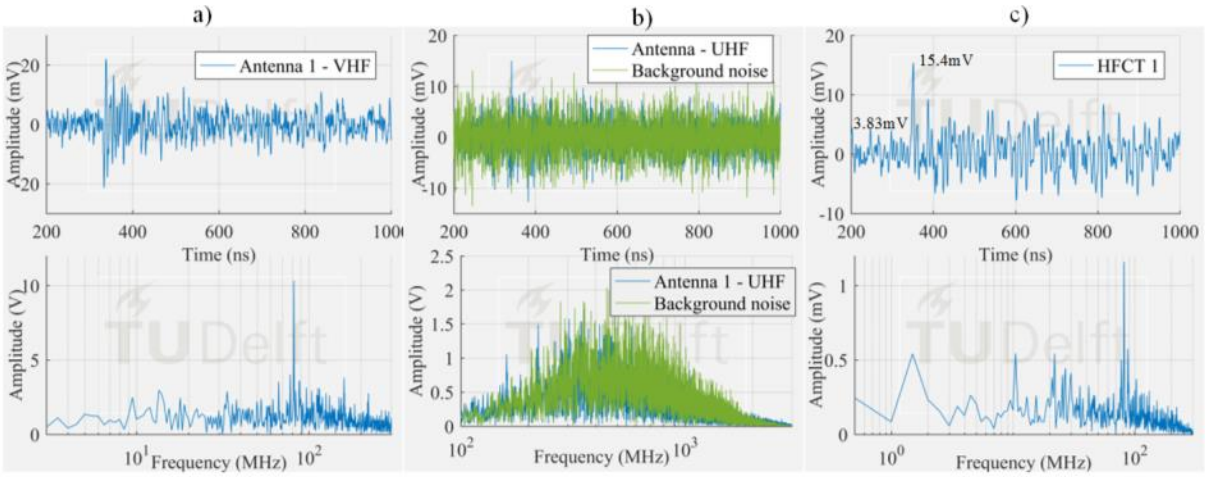

Figure 13. Smallest surface signal measured by (a) antenna 1 in VHF; (b) antenna 1 in UHF; (c) HFCT 1.

The surface test case was similar to the corona test case. The measured frequency content of the surface discharge is significant up to around 100 MHz, and as a result, the antenna 1 in VHF picked up the discharge signal but not in UHF range. On the other hand, the free particle discharge produced a frequency spectrum that extended up to 400 MHz, also with a frequency peak at 950 MHz. This broader frequency spectrum resulted in the discharge signal being picked up both in VHF and UHF range.

It is also interesting to notice that the HFCT 1 was able to pick up the discharge signal in all the three study cases. Moreover, the ratio of the peak amplitude and the background noise (peak amplitude before the starting of the pulse) was always higher than 4. This result is remarkable because the vertical range of the 8-bit oscilloscope used for the experiments was set for proper acquisition of the biggest signals, hence unavoidably coursing the digitalization of the smallest ones.

This project has received funding from the European Union's Horizon 2020 research and innovation programme under grant agreement No 691714.

The signals measured by the HFCT sensors corresponding to the largest PD discharges in Figure 9 can be seen in Figure 14 to 16. In this case of study, the signals from the HFCT 1 and HFCT 7 (located at the opposite end of the GIS 16 m away from the test cell) are reported. Before reaching the HFCT 7, the induced PD currents passed over the several components of the GIS that distorted the signals. However, the amplitude is reduced in a much less extend as evidenced by the low background noise. On the other hand, a less number of GIS components between the PD source and the HFCT sensor results in a lower pulse distortion as can be observed from the results of HFCT 1.

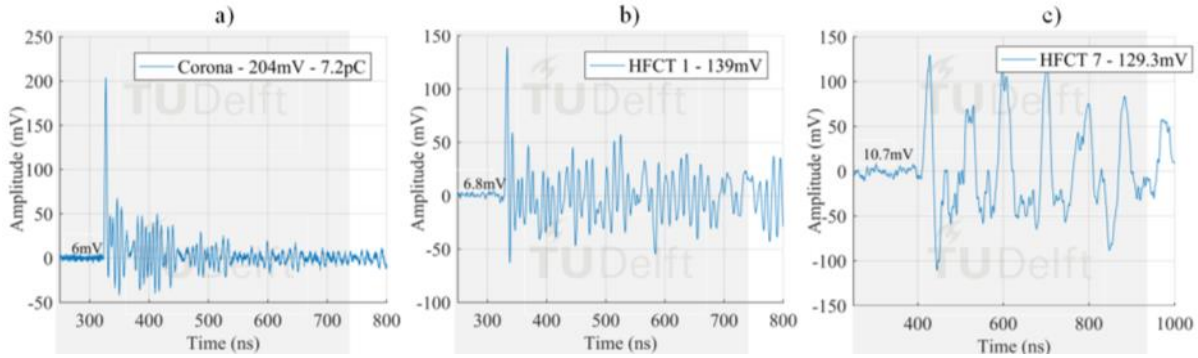

Figure 14. Largest corona signal measured by (a) Test cell HFCT; (b) HFCT 1; (c) HFCT 7.

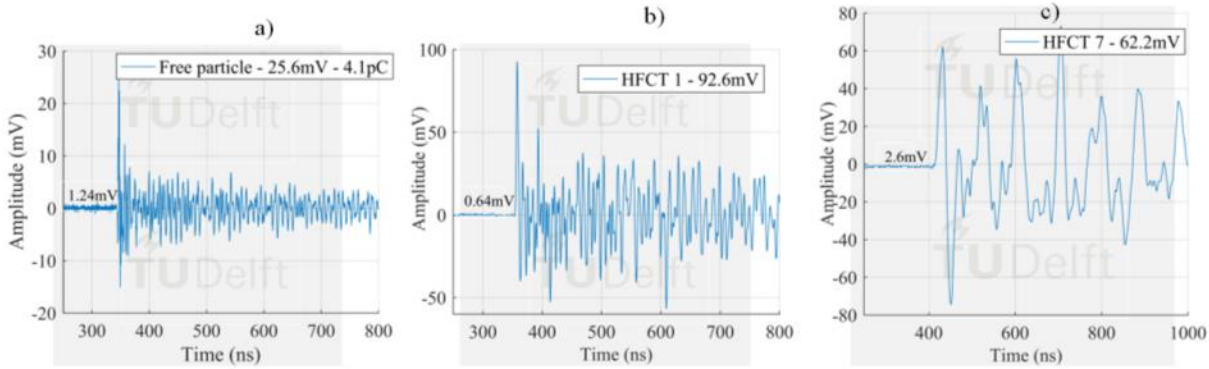

Figure 15. Largest free particle signal measured by (a) Test cell HFCT; (b) HFCT 1; (c) HFCT 7.

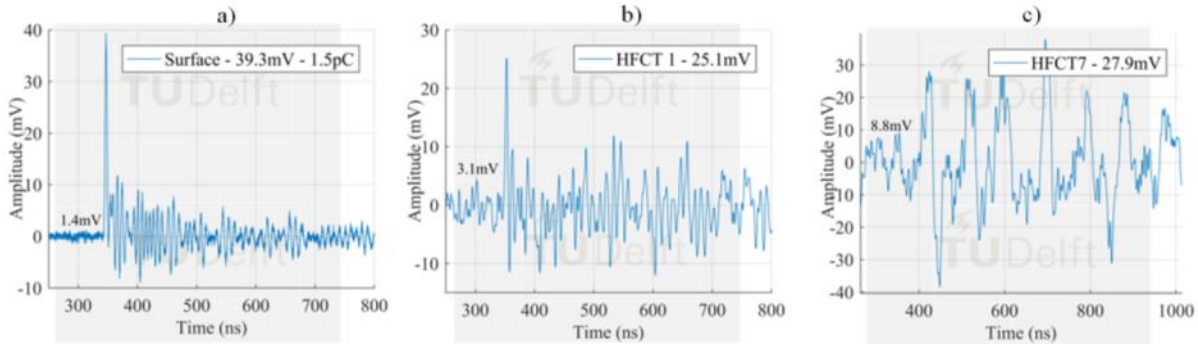

Figure 16. Largest surface **s**ignal measured by (a) Test cell HFCT; (b) HFCT 1; (c) HFCT 7.

This project has received funding from the European Union's Horizon 2020 research and innovation programme under grant agreement No 691714.

4.6 SPATIAL SENSITIVITY

In this section, additional to the signals from Antenna 1 and HFCT 1, the signals of Antenna 2, Antenna 3, Antenna 4, HFCT 3, HFCT 6 and HFCT 7 are reported in order to compare the sensitivity of the HFCT and the antennas with increased distance from the PD source..

A comparison of the spatial sensitivity between the two type of sensors is summarized in the following table. When a signal clearly distinguishable from the background noise was detected then the label “yes” was given, and the label “no” otherwise.
For the case of the measurements with antennas, digital filters corresponding to the VHF and UHF ranges were applied and the criteria aforementioned was applied to each case. However, signals from antennas in section 4.6.1 to 4.6.6 are displayed as they were acquired by the oscilloscope, i.e. unfiltered raw data.

Table 3. Comparison of the spatial sensitivity between HFCT and antennas.

	Corona		Surface		Free particle	
	Largest	Smallest	Largest	Smallest	Largest	Smallest
HFCT 1	yes	yes	yes	yes	yes	yes
HFCT 3	yes	yes	yes	yes	yes	yes
HFCT 6	yes	yes	yes	no	yes	yes
HFCT 7	yes	yes	no	no	yes	yes
Antenna 1 (VHF)	yes	yes	yes	yes	yes	yes
Antenna 1 (UHF)	yes	no	yes	yes	yes	yes
Antenna 2 (VHF)	yes	yes	yes	yes	yes	yes
Antenna 2 (UHF)	yes	no	yes	yes	yes	no
Antenna 3 (VHF)	Yes	no	yes	no	yes	yes
Antenna 3 (UHF)	yes	no	no	no	yes	yes
Antenna 4 (VHF)	no	no	no	no	yes	yes
Antenna 4 (UHF)	no	no	no	no	yes	no

From the results above, both systems performs similarly well in terms of sensitivity up to the location of HFCT 3 or antenna 2. At the location of antenna 3, the detection begins to deteriorate and depend on the frequency range, i.e. VHF or UHF. At antenna 4, the detection is almost no possible for the antenna. At this distance from the PD source, the HFCT 7 may be more affected by the background noise as in the case of the surface discharge where it was no possible the detection.

In sections 4.6.1 to 4.6.6 the time domain signals of the cases in Table 2 are shown along the location of the sensors in the GIS.

This project has received funding from the European Union’s Horizon 2020 research and innovation programme under grant agreement No 691714.

4.6.1 LARGEST CORONA DISCHARGE

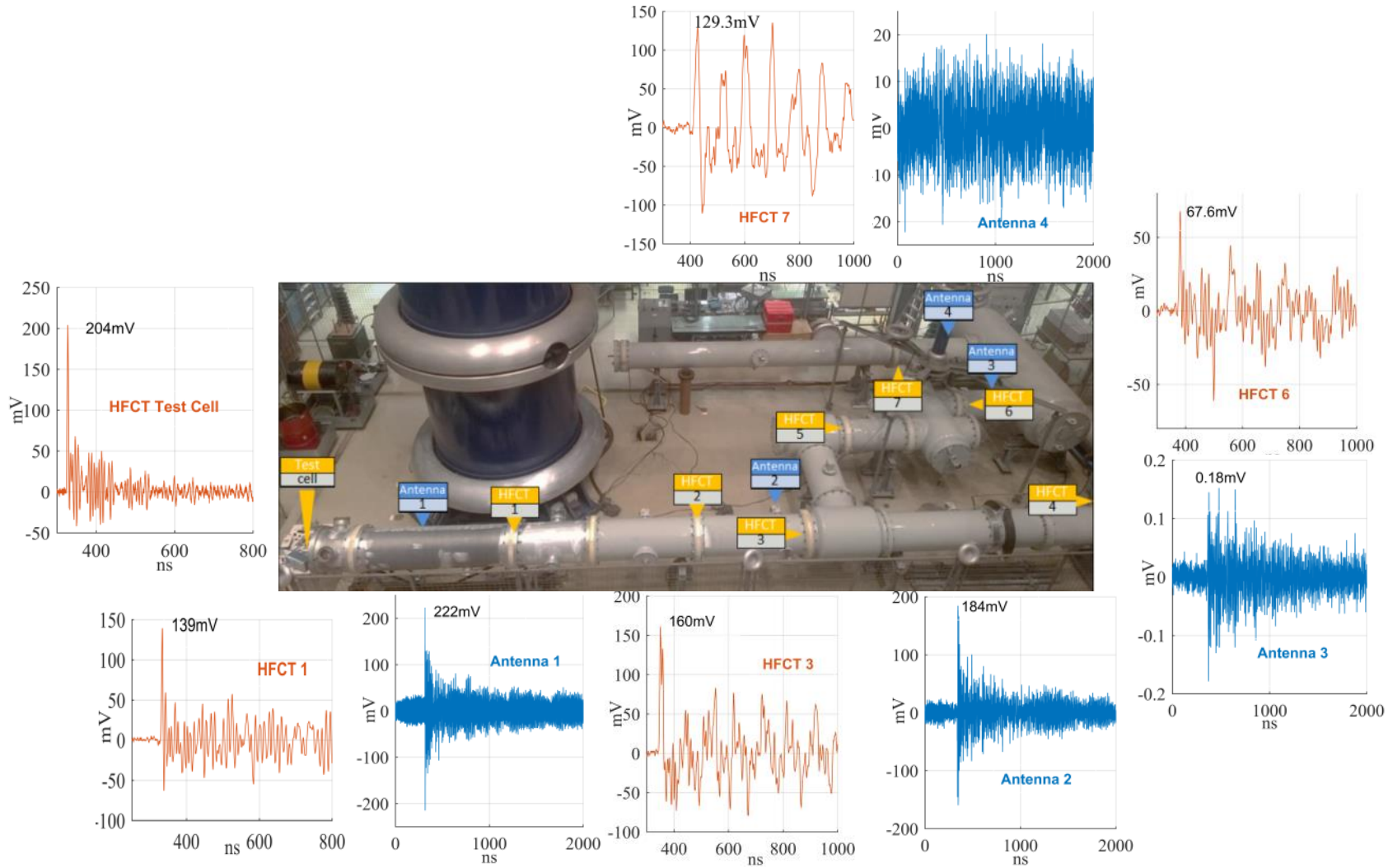

PROMOTioN – Progress on Meshed HVDC Offshore Transmission Networks

This project has received funding from the European Union's Horizon 2020 research and innovation programme under grant agreement No 691714.

4.6.2 LARGEST FREE PARTICLE DISCHARGE

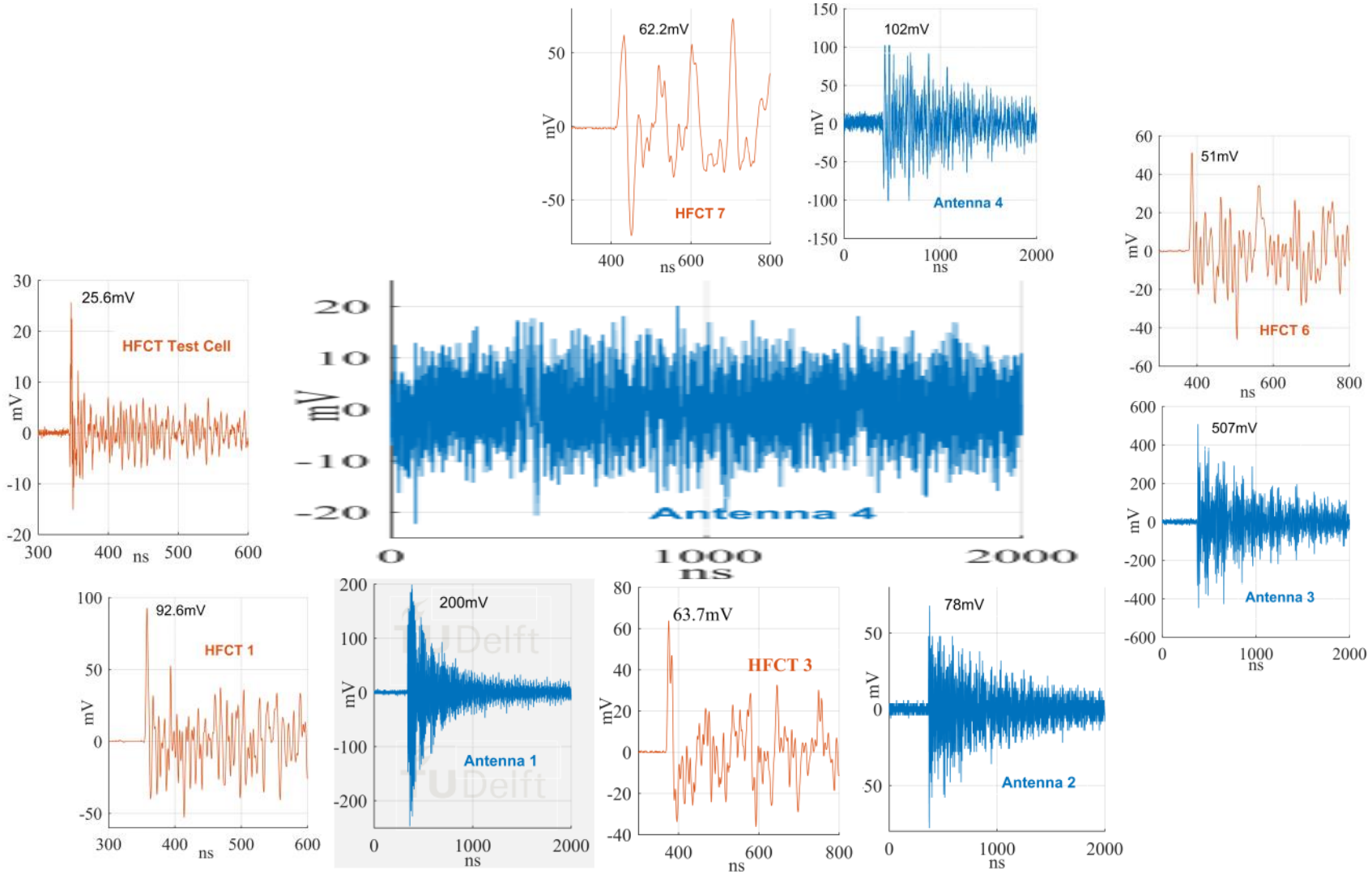

PROMOTioN – Progress on Meshed HVDC Offshore Transmission Networks

This project has received funding from the European Union's Horizon 2020 research and innovation programme under grant agreement No 691714.

4.6.3 LARGEST SURFACE DISCHARGE

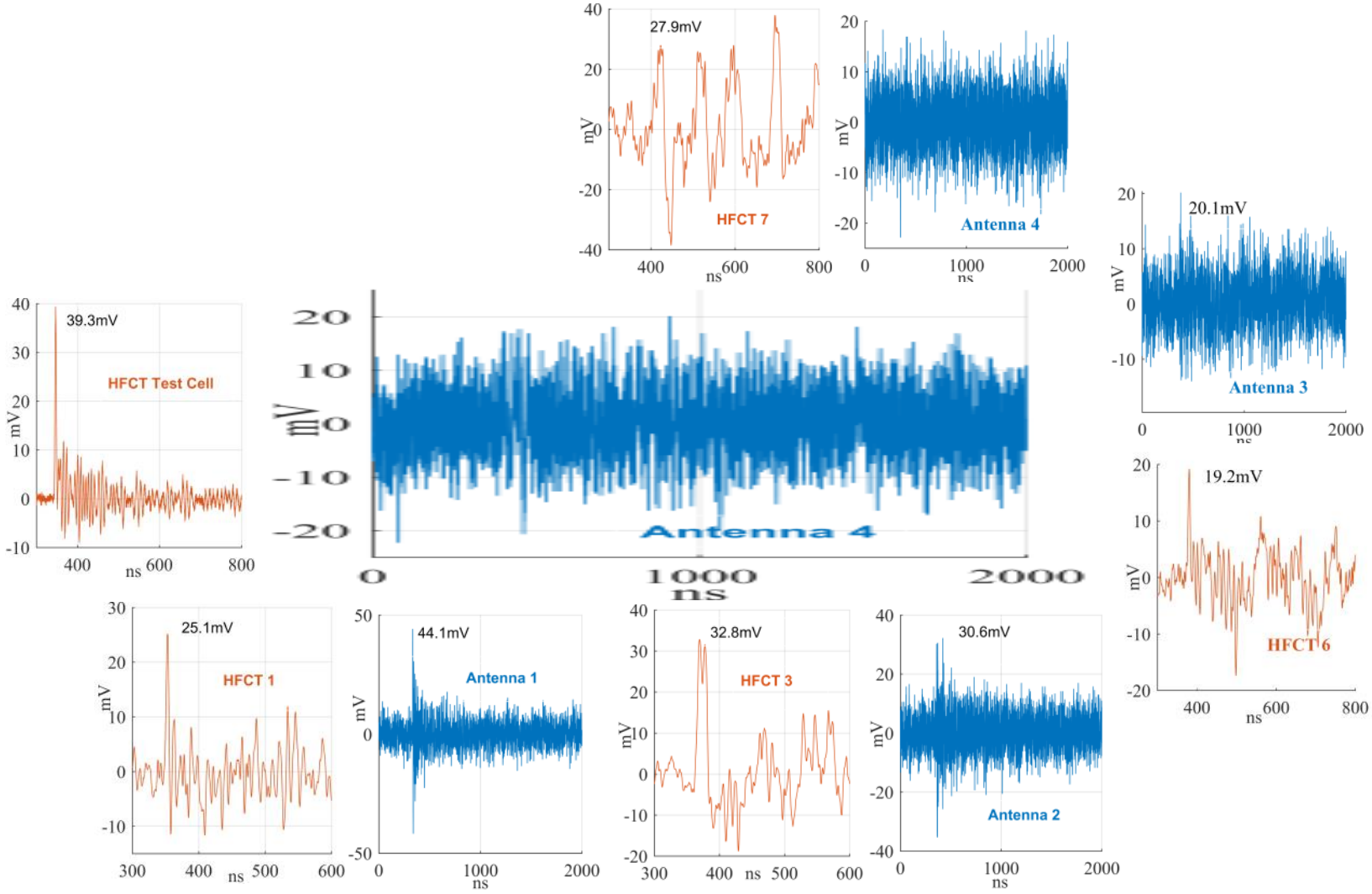

PROMOTioN – Progress on Meshed HVDC Offshore Transmission Networks

This project has received funding from the European Union's Horizon 2020 research and innovation programme under grant agreement No 691714.

4.6.4 SMALLEST CORONA DISCHARGE

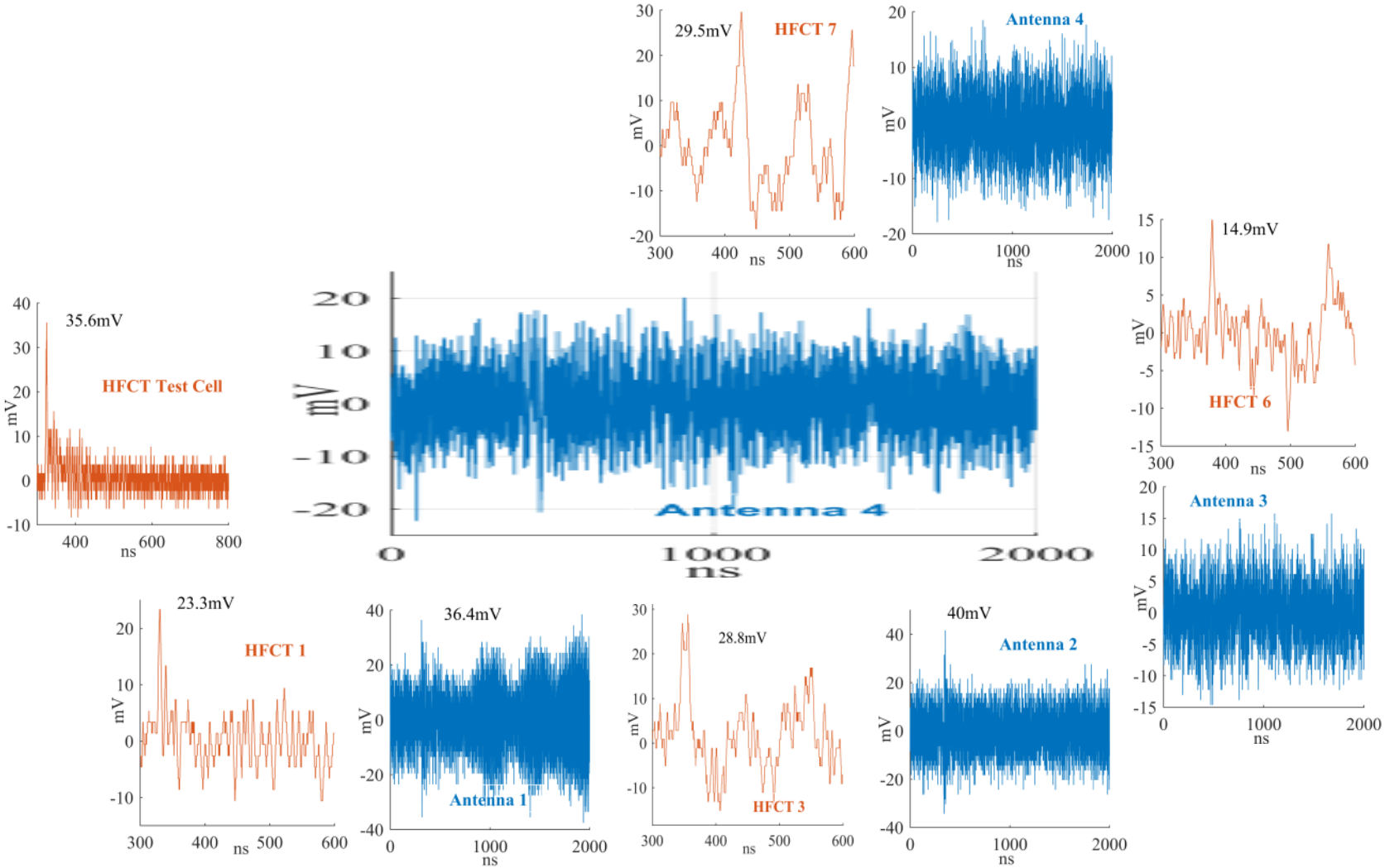

PROMOTioN – Progress on Meshed HVDC Offshore Transmission Networks

This project has received funding from the European Union's Horizon 2020 research and innovation programme under grant agreement No 691714.

4.6.5 SMALLEST SURFACE DISCHARGE

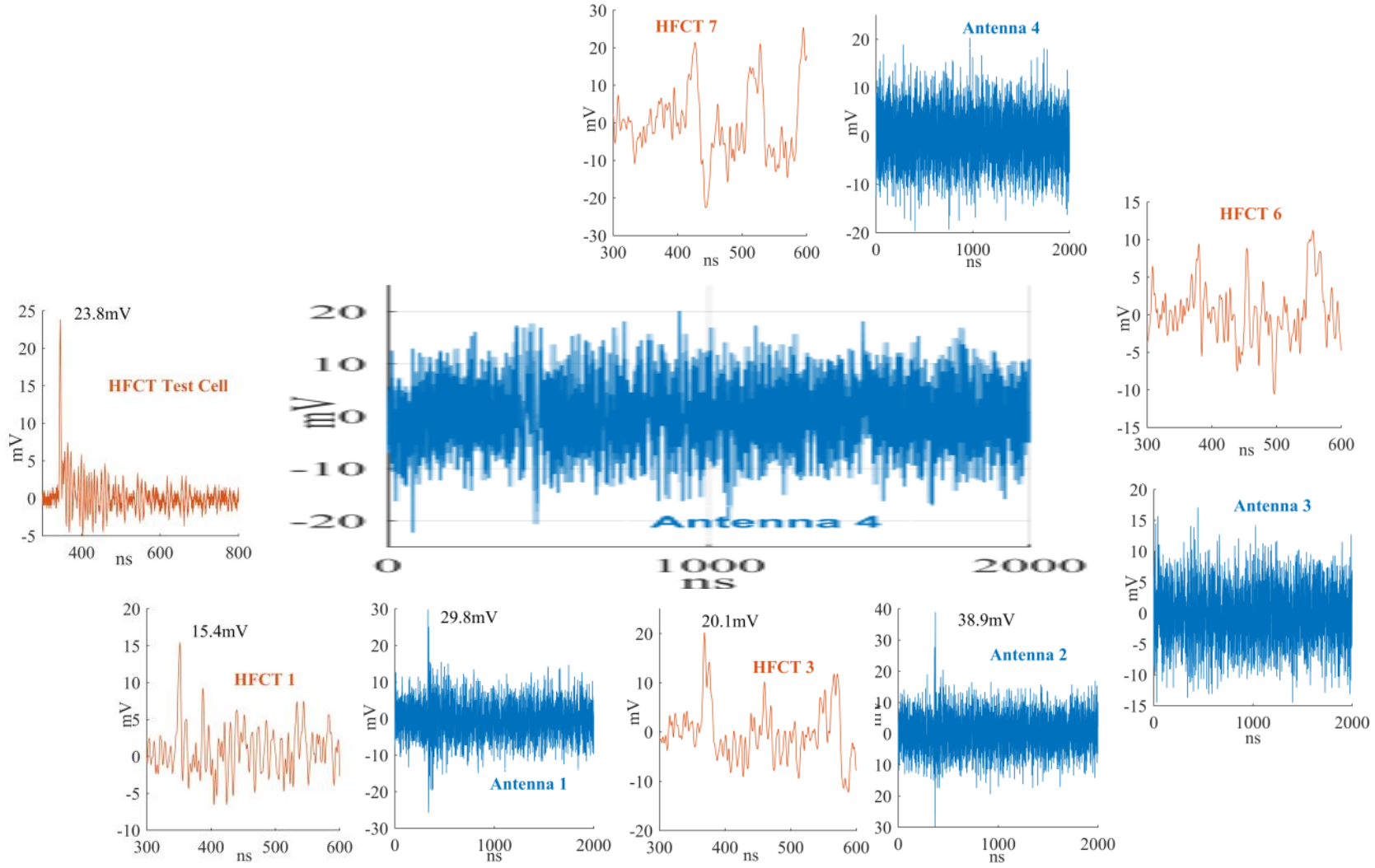

PROMOTioN – Progress on Meshed HVDC Offshore Transmission Networks

This project has received funding from the European Union's Horizon 2020 research and innovation programme under grant agreement No 691714.

4.6.6 SMALLEST FREE PARTICLE DISCHARGE

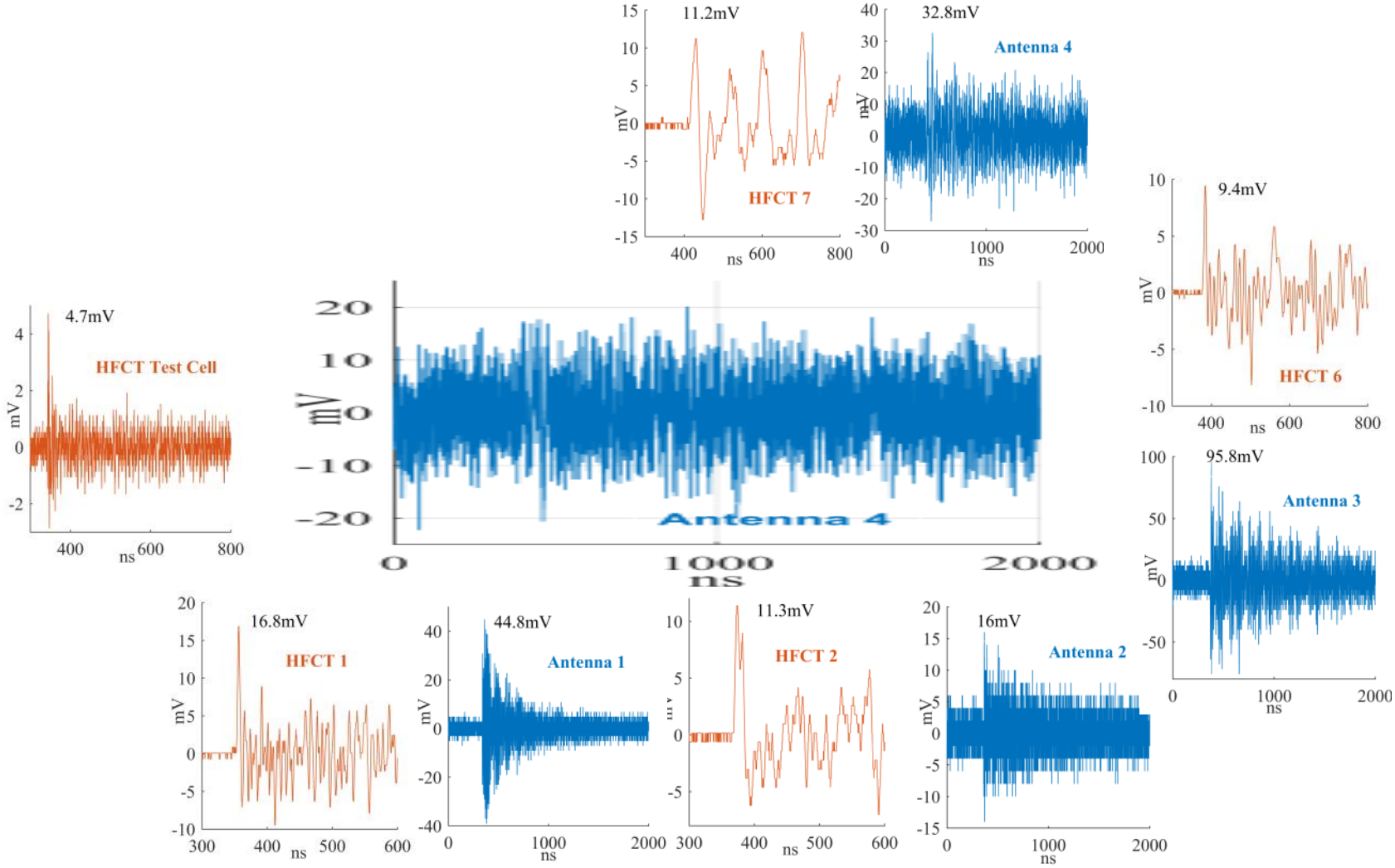

PROMOTioN – Progress on Meshed HVDC Offshore Transmission Networks

This project has received funding from the European Union's Horizon 2020 research and innovation programme under grant agreement No 691714.

4.7 ACQUISITION OF SIGNALS IN PRESENCE OF NOISE

The effect of noise on the triggering of the acquisition unit is an important matter for the performance of the HFCT-based detection system. This subject is under research and preliminary test results are included in this section.

Regarding noise, an important distintion has to be made: noise as a low value of SNR and noise as an external disturbance signal coupled to the measuring circuit leading to a false triggering of the acquisition unit. This later definition of noise is the one being researched for the purpose of this working package.

As can be seen in Figure 17, the bolt carrying the PD current is in an unshielded arrangement, therefore external disturbances may be coupled to the HFCT sensor. In order to test the effect of external disturbances an HFCT sensor was installed in one of the bolts of a short GIS provided by the partner of WP15 SuperGrid Institute in Lyon, France.

The test voltage was 70kVdc supplied by a HV DC amplifier and a protrusion in the main conductor (tungsten needle, 2cm of length and 50µm tip radius) was prepared to produce corona discharges.

Figure 17. GIS set-up to test the effect of external disturbances, fed by HV DC source.

Upon the energization of the DC source with 0V of output voltage, a big deal of radiated interference was produced by the built-in power electronics reaching a magnitude of around 12mV. Given the very low magnitude of the PD pulses produced by this particular test set up, this high level of noise made it difficult the triggering of the oscilloscope by true PD pulses.

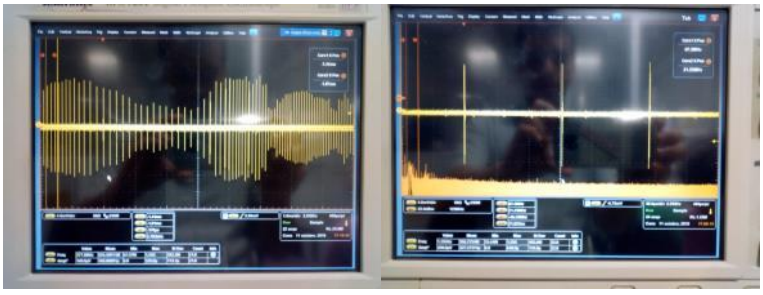

Figure 18. GIS set-up to test the effect of external disturbances, fed by HV DC source.

This project has received funding from the European Union's Horizon 2020 research and innovation programme under grant agreement No 691714.

In “sample continuous” acquisition mode was no possible to get a stable-true trigger.
However, one of the workarounds being under research is a concept that combines hardware and post-processing by software.

- Hardware. The frequency of the firing of the power electronics and the PD pulses are not synchronized and the period of a PD pulse and that of the external disturbance is also different. These two factors along with “FastFrame” acquisition mode allow for triggering the oscilloscope also on true PD signals. FastFrame or Segmentated Memory or Rapid acquisition mode is a feature becoming more and more common in oscilloscopes that enables an increased record rate. In this mode, the rearming time of the oscilloscope is so fast that PD pulses buried in between switching pulses may be still recorded.

- Software. An acquisition under heavy extermal disturbances can contain records of both PD and non-PD signals. However, the waveform of the PD pulses should be easily differenciate from the shape of non-PD pulses. Therefore, clustering techniques arise as an option for recognition of true PD signals.

A test voltage of 70kVdc was applied to the set up described above in Figure 17 and a set of 2000 pulses were recorded in FastFrame mode using an oscilloscope Tektronix DPO7354. The post-processing of the data consisted of creating cluster plots as described in [18].
Among a variety of cluster plots, the ones using the pulse features Energy/Charge vs Charge and Max Frequency peak vs Energy/Charge managed to clearly separate PD signals from non-PD signals, as indicated in Figure 19 by the data within the red circles.

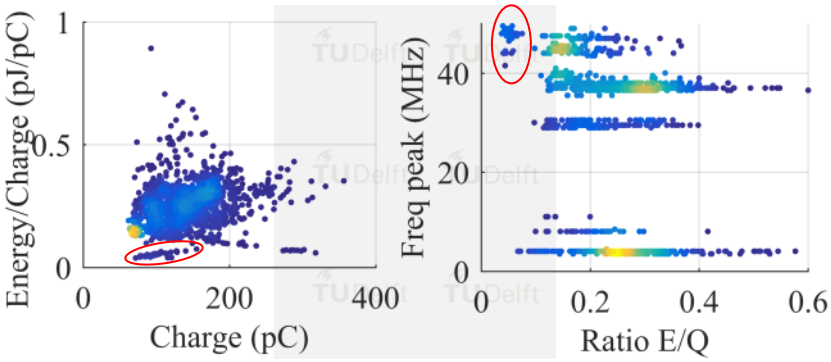

Figure 19. Cluster plots.

The software tool *PDflex* (see Section 4.8) was used to screen the waveform of the pulse corresponding to each dot in the cluster plot above and to determine the nature of each pulse.

This project has received funding from the European Union’s Horizon 2020 research and innovation programme under grant agreement No 691714.

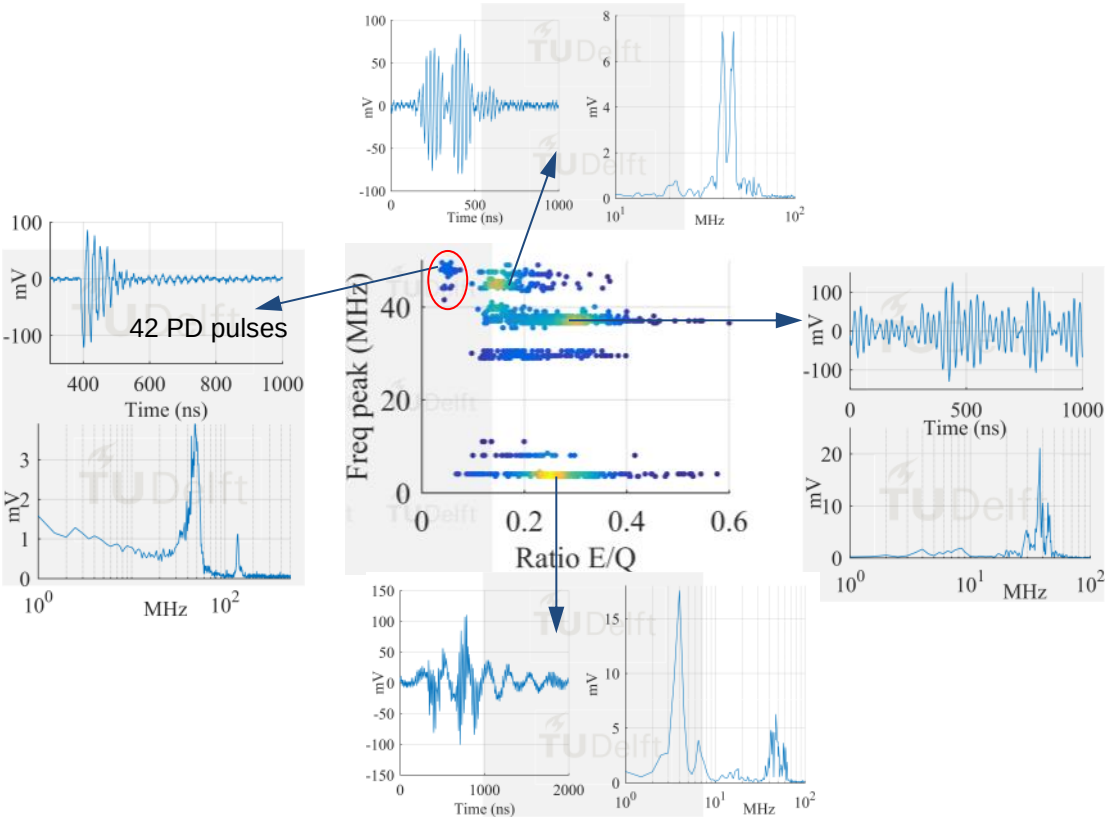

Figure 20. Waveform and frequency spectrum of a representative pulse in each cluster.

PDflex provides the option of retrieving the waveform of each dot in the cluster and its frequency spectrum. This information is useful to evaluate the shape of the pulse and its frequency content so that a PD signal can be recognize. For example, in Figure 20 the waveform and frequency spectrum of a representative pulse of each cluster is displayed. The shape of the pulses led to the conclusion that the signals within the red circle corresponded to 42 PD pulses in an acquisition of 2000 signals. Despite that the previous results proved that the detection of PD signals may be still possible even in presence of heavy external disturbances, other techniques will be further investigated in the course of the next year, which should include evaluation of:

- Gating techniques to cancel external disturbances.
- Advanced trigger functionalities, e.g. rise time trigger, mask trigger.
- Supervised and unsupervised clustering techniques.

This project has received funding from the European Union's Horizon 2020 research and innovation programme under grant agreement No 691714.

4.8 SOFTWARE TOOLS

The whole data collection in this report was acquired in time domain which meant the use of digital oscilloscopes. In addition, any PD measuring system commencially available was used. The aforementioned situation entailed that all the processing of data was to be done by our own software tools. For this purpose, two main solutions were developed: PDflex and a LabView interface.

4.8.1 PDFLEX

PDflex is software tool written in Matlab for the post-processing of digital signals acquired in time domain. This software has been made available at the website www.pdflex.tudelt.nl where user can download an executable version. Codes and algorithms are however not available.

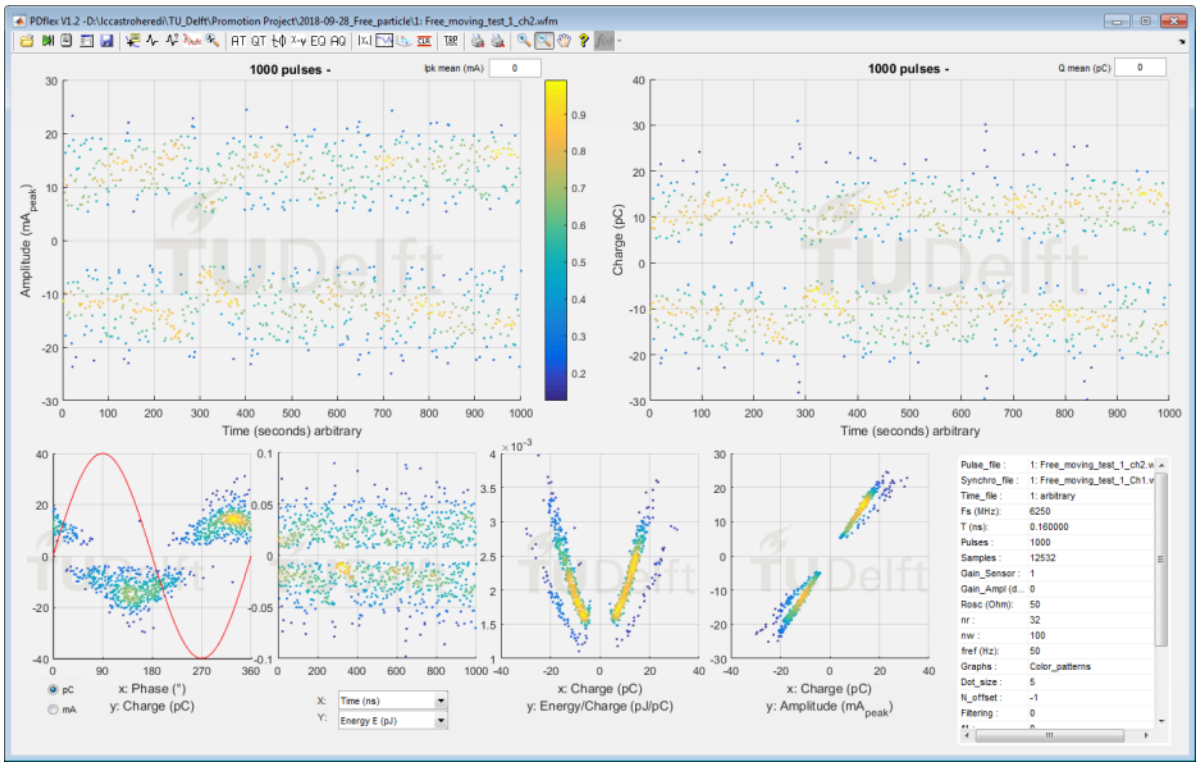

Figure 21. *PDflex* interface.

This project has received funding from the European Union's Horizon 2020 research and innovation programme under grant agreement No 691714.

Further and detailed information about *PDflex* can be found in its website along with a user manual and exemplary data. Among the functionalities of the software are:

- Interface designed for cluster visualization of data for easy reading of PD magnitudes.
- Time or Phase plots intended for DC or AC tests.
- Customizable cluster plots where the variables can be chosen from a dropdown list.
- Computation of PD parameters in time and frequency domain.
- Posibility of applying digital filters
- Browser tool. A dynamic plot that retrieves the waveform and frequency spectrum as the user hovers over the points in a cluster.
- Interactive grouping tool. In any cluster plot, the user can select points within an area of arbitrary shape and execute actions over the selected group.

4.8.2 LABVIEW INTERFACE

As part of Task 15.3, long term testing of an HVDC GIS from ABB will be carried out at Kema DNV-GL starting at the beginning of 2019. In connection with the tasks of Task 15.2, this full scale GIS was provided with 4 HFCT sensors, 2 at each lateral dismanteling unit (compensator) of the GIS, that will pick up signals during the course of the long term testing.

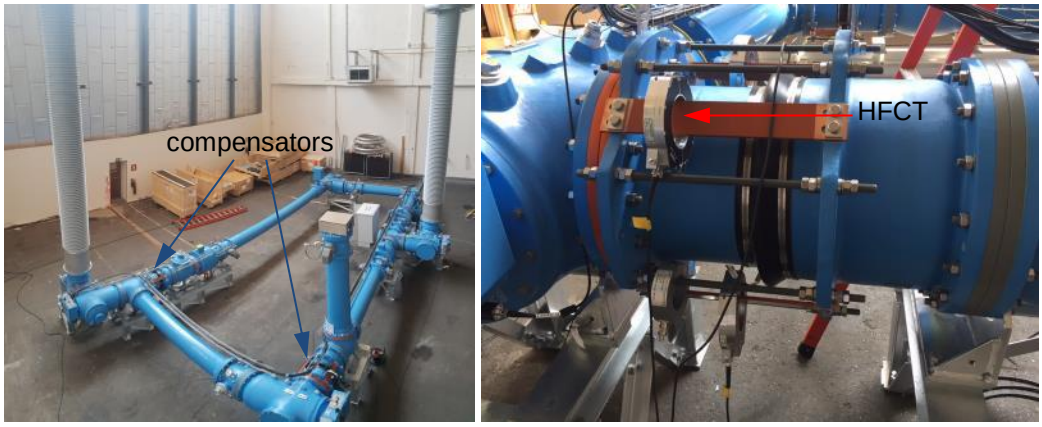

Figure 22. ABB GIS at DNV-GL.

In order to control the data acquisition and data post-processing according to the requirements of the long term testing, a Labview interface was developed considering the following features:

- **Flexibility**. Apart from the HFCT developed at TUDelft, there are many of these sensors available in the market, each of them with different characteristics, especially with different bandwidths. Consequently, the acquisition system has to be flexible enough to perform measurements with current transformers having different bandwidths. For instance, the

This project has received funding from the European Union's Horizon 2020 research and innovation programme under grant agreement No 691714.

HFCT from HVPD (see Figure 22), has a bandwidth of 100kHz – 30MHz, while the HFCT sensor developed at TUDelft has a bandwidth of 62 kHz – 136 MHz.

- **Window trigger.** The system requires to acquire the PD signals using a window trigger because it can pick-up the PD signals in both polarities.

- **Fast rearming time.** The partial discharges repetition rate is in the order of tens of µs, thus the rearming time of the acquisition system has to be less than 10 µs.

- **Fast frame.** The fast frame characteristic based on a segmented memory paves the way to capture multiple PD events with an optimized use of the memory available.

- **Semi-automatic.** For long term measurements, the acquisition system requires some degree of automatization because –under certain conditions– it is necessary to modify the acquisition parameters in order to avoid false positive PD measurements. For instance, a change in the background noise requires an adjustment in the trigger.

- **High computational capabilities.** The system has to be able to process and store a big amount of data.

To get these features, an acquisition system from National Instruments was chosen. The system consists of a PXIe 1082 chassis, a PXIe 8880 embedded controller, and two PXIe oscilloscopes.
The chassis has 8 slots and a high bandwidth backplane that allows the acquisition system to perform high-performance measurements. It also has a high-speed hard disk with a memory of 2 TB.
The embedded controller is running on Windows 7 and it has an 8 core processor, 16 GB of RAM, and Ethernet connection. These features offer high-computational capabilities, as well as a remote connection via the Ethernet port.
The two oscilloscopes are a high-speed oscilloscope NI PXIe 5162 and a low-speed oscilloscope NI PXIe 5124. The high-speed oscilloscope has four channels, a sampling frequency of 5 GS/s and an analog input resolution of 10 bits, while the low-speed oscilloscope has only two channels, a sampling frequency of 200 MS/s, 12 bits of analog input resolution, a minimum rearm time of 2 µs, and window trigger capability.
The window trigger feature of the low-speed oscilloscope allows the acquisition system to pick up the PD signals from both polarities, but it is not possible to measure signals coming from current transformers with a bandwidth higher than 50 MHz. Nevertheless, the high-speed oscilloscope has the capability to acquire the signals coming from HFCT with a wider bandwidth.
This acquisition system covers many of the features selected for the PD measuring system developed at TUDelft, for instance, the flexibility, the window trigger, the high computational capabilities, and the fast rearming time. However, the NI system itself lacks of the semiautomatic capabilities, feature that was added by means of a software application in Labview.

This project has received funding from the European Union's Horizon 2020 research and innovation programme under grant agreement No 691714.

The Labview application was built based on a state machine structure of 5 states; Initialization, acquisition, analysis, data logging, and adjust. The state machine diagram is presented in Figure 23.

At the first state, initialization, the measurement parameters for each oscilloscope are defined: the sampling frequency, the vertical range, the trigger source, the number of channels, the record length, etc. In Figure 24, the initialization state is depicted. This state also includes a previsualization of the signals that are being acquired by the HFCT sensors, which helps to identify the noise level, the PD magnitude, and waveform.

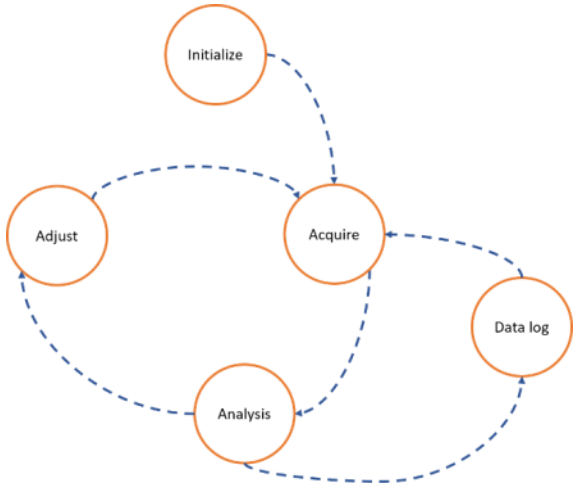

Figure 23. State machine.

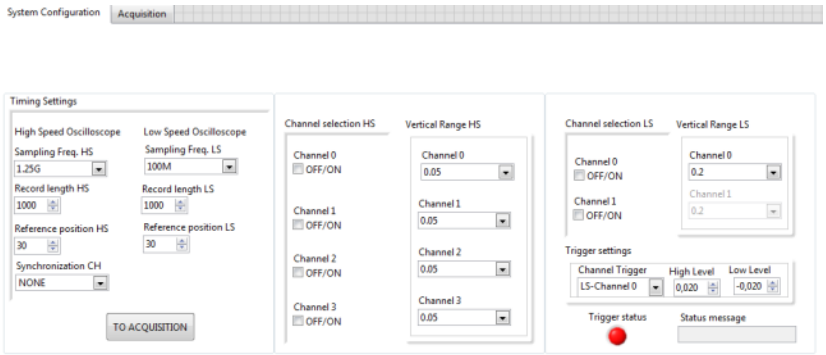

Figure 24. The initialization state.

At the acquisition state, Figure 25, the number of PD pulses to be recorded, the expected signal to noise ratio, the name of the file to log the data, and the waiting time are established. The system is able to record more than four million PD pulses because it logs the data in a cyclical way, storing a specific number of PD in a certain number of cycles; for instance, to record 100000 PD pulses, the user may set the **Number of records** at 10000 and the **Number of cycles** at 10.

This project has received funding from the European Union's Horizon 2020 research and innovation programme under grant agreement No 691714.

Figure 25. Acquisition state of the Labview application.

Another important feature of the acquisition state is the SNR expected (signal to noise ratio expected), which sets a limit to the noise level. This limit to the noise level gives way to the semiautomatic feature, that was developed at the analysis and adjust states. At the analysis stage, an equivalent of the signal to noise ratio is calculated for each cycle using the Fourier transform of the signals recorded. If the SNR is higher than the SNR expected, the system will log the data in the hard disk by means of the Data log state. On the other hand, if the SNR is lower than the SNR expected, the system will delete the signals recorded and will adjust the measurement parameters in order to perform a new measurement. The application performs the adjustment of the parameters at the Adjust state.

This project has received funding from the European Union's Horizon 2020 research and innovation programme under grant agreement No 691714.

5 CONCLUSION

In this deliverable D15.3 a partial discharge detection system for GIS was introduced. The novelty behind this system is that it makes use of HFCT sensors installed at the spacer to pick up the PD current induced in the GIS compartments.

The installation of HFCT sensors at the spacers was proven feasible to pick up the current induced by the PD events in the GIS compartments. Since the PD currents are distributed homogenously in the compartment perimeter the signal measured by the HFCT sensor might be correlated to the signal measured at the PD source. This is an outstanding result because it opens the possibility to approximate the PD magnitude in pC, which is not possible with VHF/UHF systems.

HFCT sensors properly installed at the bolts of the GIS spacers can measure PD signals with enough sensitivity. It has been demonstrated that when the HFCT is designed with a low lower cut-off frequency and wide band, the sensitivity of the system is high enough as to pick up signals far away from the PD source, leading to a high coverage of the GIS per sensor installed.

In addition, the effect of the different components of the GIS like the switchgear, T-joints, spacers, etc. decrease as the sensor is located closer to the PD source.

Other advantage obtained by this system is that a full implementation may be less expensive compared to VHF/UHF systems because the HFCT bandwidth in the range of MHz allows for lower sampling rates which can reduce the cost of the monitoring system.

In addition, the experimental results of the HFCT-based system were presented in a journal paper submitted and accepted for publication in the journal “Sensors”. Moreover, the approach of measuring the induced PD currents in the low-frequency range has led to additional measuring systems. Currently, TU Delft is working on a PD detection system that makes use of magnetic pick-up coils. Experimental results from these systems are expected to be included in the next deliverable D15.5 along with results from the long term testing of the ABB GIS at DNV-GL.

This project has received funding from the European Union’s Horizon 2020 research and innovation programme under grant agreement No 691714.

6 BIBLIOGRAPHY

1. Cigre WG. A3.06, Final Report of the 2004 - 2007 International Enquiry on Reliability of High Voltage Equipment - Part 5 - Gas Insulated Switchgear (GIS), 2012.
2. M. Hikita, S. Ohtsuka, Influence of disconnecting part on propagation properties of PD-induced electromagnetic wave in model GIS. *IEEE Trans. Dielectr. Electr. Insul.*, 2010, *vol.* 17, pp. 1731-1737, DOI: 10.1109/TDEI.2010.5658223.
3. IEC-TS-62478, High voltage test techniques – Measurement of partial discharges by electromagnetic and acoustic methods, 2016.
4. CIGRE WG. D1.25, UHF partial discharge detection system for GIS: Application guide for sensitivity verification, 2016.
5. P. V. E. Ouss, L. Zavattoni, A. Girodet, "Measurement and analysis of partial discharges in hvdc gas insulated substations," Cigre, pp. 62–69, 2018.
6. M. Florkowski, B. Florkowska, and P. Zydroń, "Partial discharge forms for DC insulating systems at higher air pressure," IET Sci. Meas. Technol., vol. Available, pp. 150–157, 2015.
7. P. H. F. Morshuis and J. J. Smit, "Partial discharges at dc voltage: Their mechanism, detection and analysis," IEEE Trans. Dielectr. Electr. Insul., vol. 12, no. 2, pp. 328–340, 2005.
8. P. Morshuis, M. Jeroense, and J. Beyer, "Partial discharge. Part XXIV: The analysis of PD in HVDC equipment," IEEE Electr. Insul. Mag., vol. 13, no. 2, pp. 6–16, Mar. 1997.
9. S. M. Neuhold, On site tests of GIS. in HIGHVOLT Kolloquium, Dresden, Germany, pp. 1–10, 2011.
10. A. Pirker, U. Schichler, Partial discharge measurement at DC voltage - Evaluation and Characterization by NoDi * pattern. *IEEE Trans. Dielectr. Electr. Insul.*, 2018, *vol.* 25, pp. 883–891, DOI: 10.1109/TDEI.2018.006742.
11. K. Mizuno et al., Investigation of PD pulse propagation characteristics in GIS. In Proceedings of Transmission and Distribution Conference and Exposition, Los Angeles, CA, USA, 1996.
12. H. Muto, M. Doi, H. Fujii, and M. Kamei, Resonance characteristics and identification of modes wave excited by partial discharges in GIS. In Eleventh International Symposium on High Voltage Engineering, London, UK, 1999.
13. CIGRE TF. 15/33.03.05, Partial discharge detection system for GIS: sensitivity verification for the UHF method and the acoustic method, 1999.
14. G. Behrmann and J. Smajic, RF PD signal propagation in GIS: Comparing S-parameter measurements with an RF transmission model for a short section of GIS. *IEEE Trans. Dielectr. Electr. Insul.*, 2016, *vol.* 23, pp. 1331–1337, DOI: 10.1109/TDEI.2015.005544.
15. A. Rodrigo Mor, L. C. Castro Heredia, Measurement system for monitoring gas insulated system. Patten application number 2018552, 2018.
16. C. Zachariades, R. Shuttleworth, R. Giussani, R. Mackinlay, Optimization of a high-frequency current transformer sensor for partial discharge detection using finite-element analysis. *IEEE Sensors Journal*, 2016, *vol.* 16, pp. 7526–7533, DOI: 10.1109/JSEN.2016.2600272.
17. A. Rodrigo Mor, L. C. Castro Heredia, F. A. Muñoz, D. A. Harmsen, A new design of a test platform for testing multiple partial discharge sources. *Int. J. Electr. Power Energy Syst.*, 2017, *vol.* 94, pp. 374–384, DOI: 10.1016/j.ijepes.2017.07.013.
18. A. Rodrigo Mor, L. C. Castro Heredia, F. A. Muñoz, Estimation of charge, energy and polarity of noisy partial discharge pulses, *IEEE Trans. Dielectr. Electr. Insul.*, 2017, *vol.* 24, pp. 2511–2521, 2017, DOI: 10.1109/TDEI.2017.006381.

This project has received funding from the European Union's Horizon 2020 research and innovation programme under grant agreement No 691714.

19. A. Rodrigo Mor, P. H. F. Morshuis, J. J. Smit, Comparison of charge estimation methods in partial discharge cable measurements. *IEEE Trans. Dielectr. Electr. Insul*., 2105, *vol*. 22, pp. 657–664, DOI: 10.1109/TDEI.2015.7076760.
20. S. Meijer. Partial Discharge Diagnosis of High-Voltage Gas-Insulated Systems, Doctoral Thesis, TU Delft, Delft, The Netherlands, 2001.
21. A. Rodrigo Mor, L. C. Castro Heredia, F. A. Muñoz, Effect of acquisition parameters on equivalent time and equivalent bandwidth algorithms for partial discharge clustering. *Int. J. Electr. Power Energy Syst*., 2017, *vol*. 88, pp. 141–149, DOI: 10.1016/j.ijepes.2016.12.017.
22. A. Contin, A. Cavallini, G. C. Montanari, G. Pasini, F. Puletti, Digital detection and fuzzy classification of partial discharge signals. *IEEE Trans. Dielectr. Electr. Insul*., 2002, *vol*. 9, pp. 335–348, DOI: 10.1109/TDEI.2002.1007695.
23. K. Rethmeier, M. Krüger, A. Kraetge, R. Plath, W. Koltunowicz. Experiences in on-site partial discharge measurements and prospects for PD monitoring. In International Conference on Condition Monitoring and Diagnosis Beijing, China, 2008.
24. A. Rodrigo Mor, L. C. Castro Heredia, F. A. Muñoz, New clustering techniques based on current peak value, charge and energy calculations for separation of partial discharge sources. *IEEE Trans. Dielectr. Electr. Insul*., 2017, *vol*. 24, pp. 340–348, DOI: 10.1109/TDEI.2016.006352.
25. R. Albarracin, G. Robles, J. M. Martinez-Tarifa, J. Ardila-Rey, Separation of sources in radiofrequency measurements of partial discharges using time-power ratios maps. *ISA Trans*., 2015, *vol*. 58, pp. 389–397, DOI: 10.1016/j.isatra.2015.04.006.

[1] F. N. L. Name, Test Test Test, Berlin, 2016.

This project has received funding from the European Union's Horizon 2020 research and innovation programme under grant agreement No 691714.